Journal of Power Sources 507 (2021) 230072

Contents lists available at ScienceDirect

Journal of Power Sources

journal homepage: www.elsevier.com/locate/jpowsour

Electrocatalysts for the oxygen evolution reaction in alkaline and neutral media. A comparative review

Michaela Plevová, Jaromír Hnát, Karel Bouzek *

University of Chemistry and Technology, Prague, Department of Inorganic Technology, Technická 5, 166 28, Prague, 6, Czech Republic

HIGHLIGHTS

- Addresses alkaline water electrolysis, a key technology in the decarbonizing society.
- Classifies the materials reported into groups according to chemical composition.
- Evaluates published data critically allowing readers to form their own judgement.
- Provides a brief theoretical background to the parameters used for a comparison.
- Proposes criteria for a comparison of the materials reported in the literature.

ARTICLE INFO

Keywords:
Oxygen Evolution
Electrocatalysis
Alkaline
Neutral
Water electrolysis

ABSTRACT

Hydrogen can be produced in a clean way from water by its electrochemical splitting. Water electrolysis consists of two half-reactions, of which the oxygen evolution reaction (OER) is the major source of energy loss. In the case of the alkaline water electrolysis, the spectrum of materials that are stable under the conditions of the OER is significantly broader than in the case of an acidic route. This review compares systematically different materials classes based on reported overpotential at current density 10 mA cm^{-2}. Plethora of studies was gathered to accomplish this task and the OER catalysts reported in the literature to date are summarized. In addition, we have provided an insight into the catalyst activity descriptors allowing theoretical identification of the most active materials. In order to assist the reader in gaining a better understanding of this complex subject, the catalysts are classified into three main groups in agreement with their chemical composition as transition metal oxides, phosphides and selenides. Less frequently used materials are reported in a separate group. Near-neutral or neutral pH conditions are considered as well.

1. Introduction

Nowadays, there is a growing interest in reducing greenhouse gases and other air pollutants (NO_x, SO_x, fine particulates) emissions. Consequently, there is a need for renewable energy sources, such as wind and solar, to be incorporated into the electricity distribution grid. One of the main problems is the intermittent energy supply from these sources and their seasonal variations. One solution to this problem is the possibility of energy conversion and storage, thus allowing load-levelling. Hydrogen (H_2) production by means of water electrolysis represents a viable option to fulfil this task [1]. There are three types of the water electrolysis technologies, differing in operating temperature and in the electrolyte used. In the low temperatures range, we distinguish two technologies, namely alkaline water electrolysis (AWE) and proton exchange membrane water electrolysis (PEM WE). The AWE is operating at temperatures between 60 and 80 °C with 30 wt% KOH water solution as an electrolyte reaching produced H_2 purity of 99.9%. Recently, focus is on development of a membrane alternative of the alkaline water electrolysis, utilizing anion selective membrane as an electrolyte and separator in one. Here the target is to replace KOH solution by demineralised water as a circulating medium [2]. PEM WE operates at 50–80 °C with pure water as a circulating medium. Ionic conductive contact is secured by means of a proton selective perfluorinated sulphonated polymer in a form of a membrane and catalyst layer binder. Produced H_2 has a purity of 99.99% after drying. The high temperature process is represented by the solid oxide water electrolysis (SOWE)

* Corresponding author.
E-mail address: Karel.Bouzek@vscht.cz (K. Bouzek).

https://doi.org/10.1016/j.jpowsour.2021.230072
Received 9 March 2021; Received in revised form 4 May 2021; Accepted 19 May 2021
Available online 4 June 2021

operating typically around 800 °C utilizing zirconia ZrO_2 stabilized with yttrium oxide as an electrolyte. High temperature reduces the electricity consumption but a part of the energy must be supplied in the form of thermal energy [3]. Hydrogen produced this way can be used for electric power recovery, e.g. by means of hydrogen powered fuel cell, when the renewable energy is not available [1]. Besides this, the green H_2 produced by water electrolysis can also be used as the fuel for fuel cell-powered electric cars, or as a raw material for industry. However, as with most electrochemical energy technologies, the cost, efficiency, reliability, and lifetime must be optimized to satisfy market requirements [4]. The electrolysis of water is a technology used since the turn of the 19th and 20th centuries. This was an alkaline technology and it utilized aqueous hydroxide solutions as an electrolyte, as it still does today. Currently, however, the demands for this technology are to produce pure hydrogen and oxygen at low overpotential, thus reducing the energy requirements. In terms of operating cost, water electrolysis will always require more energy, as ~238 kJ is needed to produce 1 mol of H_2 from water, while only ~41 kJ is needed to extract 1 mol of H_2 from methane by steam reforming process under standard conditions. A possibility of energy consumption reduction lies in the replacement of the liquid electrolyte and production of hydrogen, for example, via glycerol electrolysis using $Ni(OH)_2$ as an anode catalyst. Here, the thermodynamic limitations of water electrolysis are overcome by replacing the anodic oxygen evolution reaction with the oxidation of more easily oxidizable glycerol, which significantly decrease the reaction potential (about 240 mV). Also, valuable oxidation products can be obtained (glycerate, carbonate, formate, glycolate, tartronate, mesoxalate, lactate or oxalate ions) [5]. But only a very limited number of studies was published regarding the electrochemical oxidation of glycerol as the intensity of the process is rather low [6]. Nevertheless, the advantage of water electrolysis is the compactness, possibility of powering by renewable power sources and thus to produce carbon dioxide (CO_2) free H_2, which will prevail in the future [7].

In order to fulfil low overvoltage requirement, electrocatalysts represent a critical aspect in terms of enhancing the reaction rates and selectivity control of electrochemical reactions, such as H_2 evolution and oxidation, oxygen (O_2) evolution and reduction, and CO_2 reduction. These reactions are necessary for electricity generation in fuel cells, H_2 production through water electrolysis, and CO_2 conversion into "green" fuels and chemicals.

Electrolytic water splitting is the topic of this review. It consists of two half-reactions, including the hydrogen evolution reaction (HER) and the oxygen evolution reaction (OER). HER catalysts have been extensively studied by many research groups. Based on the review published recently by our group [8] we can sum up the main findings about HER catalysts. Platinum-group metals are the most active materials in a wide range of pH, but their high price and scarcity forces the researchers to search for non-precious alternatives. In an alkaline environment, Fe and Fe-based alloys have relatively low HER overpotential (200 mV overpotential at current density 10 mA cm^{-2} (η_{10})). The promising material based on Fe seem to be Fe–Mo–Ni alloy. Co-based catalysts are another group suitable to replace the Pt-group metals. Again, Co–Ni–Mo alloy seems to be the best from this group. Ni-based materials are the third main group with the alloy of Ni and Mo being the benchmark of non-platinum catalysts. $MoNi_4/MoO_2$@Ni reached only 15 mV at η_{10}. In neutral media, nitrogen-modified porous Ni framework reached only 64 mV at η_{10}. Similar results were achieved with hollow nanoparticles of Co nanocrystal. Besides alloys, materials such as sulphides, selenides, nitrates, carbides and phosphides are also studied. These materials are usually combined with Ni, Mo and Co. The promising materials here are MoS_2 supported on carbon [9] or two-dimensional Mo_2C [10].

The transfer of four electrons is necessary per oxygen molecule evolved. The OER is thus clearly the more complex reaction. Consequently, due to the sluggish kinetics requiring a high amount of energy to overcome the activation barrier [11], it is mainly responsible for the inefficiency of the water electrolysis cell [12]. Therefore, in the case of the OER, there is a lot of scope for efficiency improvement by means of a suitable catalyst. An efficient catalyst for the OER should be able to operate in a broad pH range, at low overpotentials with high current densities, over an extended period of time (from years to a decade) and should be prepared from earth-abundant materials by a simple and cost-effective method [13]. With respect to these demands, first-row transition metal compounds, such as Co-, Ni-, and Fe-based materials, have been extensively investigated as efficient electrocatalysts for this reaction [14].

These types of materials are, however, not stable in an acidic environment, where usually precious metal and precious metal oxide-based catalysts must be used. Compared with an acidic environment, water electrolysis in alkaline media allows the utilization of earth-abundant materials, which reduces the cost of the entire device [15]. Concerning the electrocatalysts for the OER in alkaline media, much work has focused on different materials with different structures and properties. Moreover, the catalyst testing protocol varies significantly among the individual authors, therefore a comparison of all these materials is complex. The aim of this paper is to sift, compare and suggest promising materials on which future work can be focused.

2. Oxygen evolution reaction (OER)

In an alkaline environment the OER is usually written as:

$$4\ OH^- = 2\ O_2 + 2\ H_2O + 4\ e^-\ E^0 rev. = 0.401\ V\ (25\ ^\circ C,\ pH\ =\ 14) \quad (1)$$

This is, however, only an overall equation that does not concern the reaction steps in the mechanism. Generally, the OER can be described as a four-step process, represented by Reactions 2–5b. These reactions describe generally OER process in which each step can be modified according to the studied catalyst. Thus, more reaction paths can be recognized [16]. Reaction 2 consists of the formation of M − OH via the one-electron oxidation of hydroxide anions adsorbed on the catalyst active site (M; does not necessarily mean metal atom/site). In Reaction 3, M−OH transforms into M−O after a couple of protons and electron have been removed. Then, two different paths of O_2 generation are possible. The first path is described by Reaction 4, where two M−O species recombine under the formation of the O_2 molecule and two free M active sites. The second path is described by Reactions 5-a,b, where M−O converts into M–OOH after it merges with hydroxyl anion under one-electron oxidation (Reaction 5a). Subsequently another proton-coupled electron transfer process proceeds, producing the O_2 molecule and the initial active site (Reaction 5b) [15].

$$M + OH^- = MOH + e^- \quad (2)$$

$$MOH + OH^- = MO + H_2O + e^- \quad (3)$$

$$2\ MO = 2\ M + O_2 \quad (4)$$

$$MO + OH^- = MOOH + e^- \quad (5a)$$

$$MOOH + OH^- = M + O_2 + H_2O + e^- \quad (5b)$$

All the reaction intermediates are bound to the surface as peroxo or oxo compounds. The activation barriers between these intermediates and their relative stabilities affect the rate-determining step (RDS) as well as the general rate of the OER. The properties of these surface intermediates depend on the reaction conditions and the catalyst material [11,17,18].

The difference between the chemisorption energies of two sequential intermediates is equal to the change in Gibbs free reaction energy, ΔG, of the elementary step at a stated electrode potential. On the premise that the overall reaction must be exergonic (i.e. ΔG has to be negative) the minimum electrode overpotential could be predicted [19,20]. In Fig. 1, volcano plots for different materials are shown with the universal

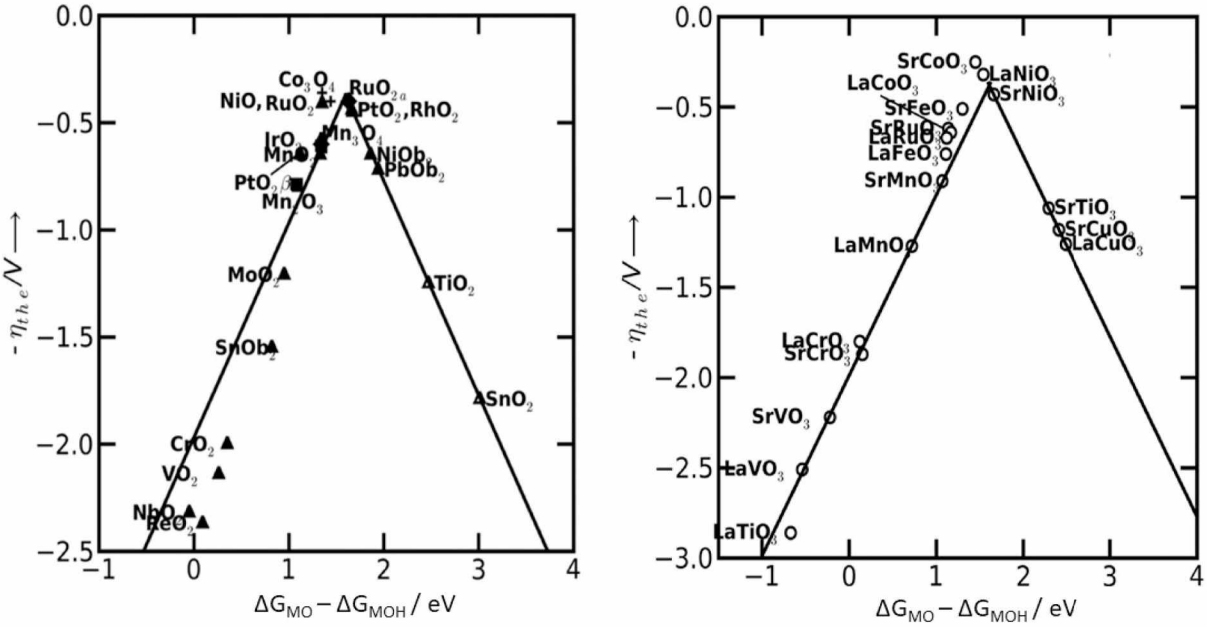

Fig. 1. Volcano plot revealing η_{the} vs. the difference between the standard free energy of two intermediates ($\Delta G_{MO} - \Delta G_{MOH}$) for various binary oxides (left) and perovskite oxides (right). η_{the} stays for linear correlation with experimental η_{10} for single class of materials [30]. All experimental values were recorded at room temperature and pH 14. Reprinted with permission from Ref. [30]. Copyright 2011 John Wiley and Sons.

activity descriptor for the OER being the difference in the energies of MO and MOH ($\Delta G_{MO} - \Delta G_{MOH}$) [21]. This activity descriptor is used due to the linear scaling relation between the free energies of MOH and MOOH ($\Delta G_{MOOH} = \Delta G_{MOH} + 3.2 \pm 0.2$ eV). This scaling relation constitutes the launching point to construct an overpotential-dependent volcano plot for the OER over transition-metal oxides [21,22]. The deviation in the offset (±0.2 eV) usually depends on a function of the exchange correlation functional used in the DFT calculations or on the class of materials. Concerning the DFT calculations, there is growing awareness about the influence of solvation in scaling relations and volcano plots. Recent studies highlight the importance of solvation for the realistic modelling of electrocatalysts. Utilization of Frost diagrams (the free energy vs oxidation state of a chemical species; it illustrates the relative stability of a number of different oxidation states of a particular substance depending on pH) requires identifying the free energy of intermediate solution species. For OER, the important solution species are OOH^- (aq) and OH^- (aq) as the difference of Gibbs energies of these two species (ΔG_{OOH^-} (aq) – ΔG_{OH^-} (aq)) are equal to difference of the free energies of MOH and MOOH (ΔG_{MOOH} - ΔG_{MOH}) [23].

The shortcoming of the conventionally applied activity descriptor (ΔG_{MOOH} - ΔG_{MOH}) is that it relies on the evaluation of free-energy changes at zero overpotential, thereby taking only the highest free-energy change among the mechanistic description into account, which can be unfavourable for detailed approximation of the electrocatalytic activity [27]. One of the possibilities of more precise prediction of the activity of OER catalyst is the electrochemical-step symmetry index (ESSI), which can be determined regardless of the presence or absence of adsorption-energy scaling relations between intermediates [28]. Another activity descriptor represents $G_{max}(\eta)$, which contains information on the kinetics and applied overpotential in its framework. $G_{max}(\eta)$ is given by the transition from the active metal site to the OOH adsorbate, thereby approaching the rate-determining step and revealing linear dependence with experimental data across various material classes [27]. The linear scaling relationship is based on DFT calculations and is considered to be the current state-of-the-art in electrocatalytic activity predictions. It can describe the leg of volcano curve precisely but loses its precision in the volcano's top, where microkinetic details need to be considered. So, this method can be improved by introducing kinetic scaling relations and overpotential-dependent volcano plots. In this case, rate-determining step is considered as well as the overpotential, which is required for the description of the volcano's apex. Moreover, ESSI can be used as more sensitive activity descriptor. The goal is to combine those methods and obtain an overall and more credible description of catalytic activity [29].

The volcano plot is based on the Sabatier principle. It describes the presumption for a high reaction rate as not too strong, nor too weak binding of intermediates to the catalyst active site. A principal difficulty with the volcano plot is the lack of reliable information, because the values obtained by different groups on similar systems differ widely. Therefore, it must be pointed out that the volcano plot is most often theoretical for OER due to the scaling relations [24–26].

At the top of the volcano plot are materials with a minimal theoretical overpotential towards the OER [30]. The OER occurs at a suitable reaction rate on noble metal oxides (e.g., IrO_2, RuO_2). RuO_2 exhibits high catalytic activity towards the preferred reaction. Due to its significantly better corrosion stability, however, IrO_2 represents the state-of-the-art catalyst [31–36]. The higher OER activity of RuO_2 corresponds to its optimum bonding strength to the OER intermediate species from a thermodynamics standpoint [37]. However, based on the data from the volcano plot, first-row transition metal compounds, such as Co-, Ni-, and Fe-based materials, also represent a suitable and efficient option for electrochemical water splitting catalysis [14]. Their multivalent oxidation states ($M^{2+}/^{3+}/^{4+}$; M = active site, which does not have to be metal atom) are responsible for their excellent OER activity. It has been confirmed that M^{4+}-containing species are the catalytic sites for Co based catalysts, while M^{3+} species are the active sites for Fe and Ni [38]. Furthermore, their OER activities highly depend on the composition, the morphology, the electron number of the transition metal and the surface binding energy of oxygen [39]. This means that there are many possibilities for modification of both the physical (roughness factor, conductivity) and the chemical (oxidation state) properties of the materials. These modifications can be achieved by doping, the fabrication of binary oxide mixtures or by increasing the electrochemically active surface areas [40].

All these modifications and their influence on catalytic activity will be discussed in the next chapters focused mainly on the three most active

OER catalyst groups, namely oxides, phosphides and selenides. These groups of materials are most widely studied in the literature. Most of the papers published differ according to the dopants or preparation methods used. In this review, all these variations will be summarized, and the activity of the materials compared based on the overpotential they show at a current density of 10 mA cm^{-2} (η_{10}). This value is low with respect to the desired industrial application, where current densities higher by 1 or 2 orders of magnitude are foreseen. Nevertheless, it is the value commonly used to compare different materials. This value is used as it is in the range, where electrode reaction kinetics is influenced mostly by the catalyst properties without important impact of different parameters, e.g. vigorous gas evolution causing irreproducible shielding of the electrode surface as well as variation of the ohmic potential drop making thus result subject of higher experimental error. Overpotential generally represents the difference between the applied electrode potential (E) and the electrode potential under equilibrium conditions (E_{eq}) [11]. Overvoltage was chosen as a parameter for comparison as it represents the main parameter describing the kinetics of the electrode reaction. A current density value of 10 mA cm^{-2} was selected due to the fact that most of the authors report the overvoltage value at this current load. Thus, different materials can be compared relatively easily [41].

3. Oxides

Metal oxides are more thermodynamically stable under oxidizing potential than other compounds, such as sulphides, selenides, nitrates, etc. [42]. Typically, they are divided according to their most common crystallographic structure into two main groups, namely spinels and perovskites. In the case of spinel-type materials with the general formula AB_2O_4, the oxygen ions form a cubic, close-packed structure with eight tetrahedral and four octahedral sites per formula unit. Perovskites have the general formula ABO_3 with a cubic structure which is rarely encountered. The orthorhombic and tetragonal phases are the most common non-cubic variants [43]. Both structures will be discussed in the following chapters in detail.

3.1. Spinels

The activities of oxidized Ni, Co and Fe metals towards the OER were compared by Lyons et al. [44]. Their catalytic performance, based on a comparison of the overvoltage, decreased in the following order: Ni > Co > Fe. The catalytic activity for the OER is possibly related to the OH–$M^{2+\delta}$ bond strength ($0 \leq \delta \leq 1.5$) with the order of Ni < Co < Fe, i.e. inverse to that of the activity. When Ni is oxidized, the transition from Ni^{2+} to Ni^{3+} occurs ($Ni(OH)_2$ to NiOOH). The decrease in overpotential with an increasing amount of NiOOH suggests that Ni^{+3} is the active centre. For this reason, the performance of Ni is even further improved after electrochemical ageing, where more Ni^{3+} is formed. When Co is oxidized, the transition from Co^{2+} ($Co(OH)_2$ or CoO phases) to Co^{3+} and Co^{4+} occurs, which is also beneficial for OER activity [45]. The oxidation of Fe begins with the formation of Fe^{2+} (FeO or $Fe(OH)_2$), which is followed by Fe^{2+}/Fe^{3+} redox transition with the structure $[Fe_2O_3(OH)_3(OH_2)_3]_3$, followed by the formation of Fe^{3+} species (Fe_2O_3, FeOOH and Fe_3O_4), and then further to oxo ligands which can reach a higher oxidation state than +3 [46,47]. The binding energy of the OH–$M^{2+\delta}$ bond can also be altered by combining the metal oxides with other elements [48,49]. It was proposed that a high-oxidation-state Fe species might be the active site in combination with Ni [47] as Fe can reach a higher oxidation state [Fe^{4+}, Fe^{5+}, Fe^{6+}] than Ni [Ni^{3+}] at potentials relevant to water oxidation in alkaline media.

3.1.1. Fe-based spinels

Of the three transition metals mentioned above, Fe is the most abundant and as such it is a highly attractive element for application as a low-cost OER catalyst [14]. The drawback of Fe and Fe-doped catalysts lies in their lower activity towards the OER compared to Co-based catalysts [50]. However, it was proposed that differences in activity among the different metals may, apart from other factors, be caused by structural differences and available surface areas [50]. Due to this, the structure of Fe-based catalysts can be altered by synthesis, which could narrow the gap in performance observed between Fe and other transition metal oxides [38]. For example, hierarchical hollow nanoprisms of Ni–Fe layered double hydroxide (LDH) have a high specific surface area of 245 $m^2 g^{-1}$ and high catalytic activity with overpotential for the OER of only 280 mV at 10 mA cm^{-2} (1 M KOH, 25 °C) [51]. Other beneficial structures include, for example highly oriented flake array structures [50] or nanosheets [52] uniformly grown on the surface of the substrate.

A simple Fe_3O_4 catalyst reached η_{10} of 438 mV (1 M KOH, 25 °C) [53]. A satisfactory performance of a Fe-based catalyst was proven for spinel structures (AB_2O_4). Transition metal ferrites with a general formula of MFe_2O_4 (M = Co, Ni, Cu, etc.) make up an important part of this group with many interesting properties, such as rich redox chemistry, high electric conductivity, low toxicity, simple preparation and low cost [54]. Usually, the MFe_2O_4 spinel oxide has an inverse spinel structure in which oxygen is in the face centered cubic (fcc) phase with M^{2+} occupying the octahedral (O) site and Fe^{3+} distributed uniformly in the octahedral and tetrahedral (T) sites, as shown in Fig. 2. Such a structure has shown great electrical conductivity due to electron hopping between various valence states of metals in octahedral sites [53]. Due to the bimetallic nature of spinel, the conductivity of ferrites can be altered by replacing them by a different metal. This is because the electrical conductivity of ferrites originated from the above-mentioned electron hopping, resulting in redox changes between Fe^{2+} and Fe^{3+} ions [55]. In the sintering procedure, some lattice oxygen can escape from the oxide, causing an oxygen shortage in the crystal lattice. Therefore, to even the electrical charge produced in the lattice unit, Fe^{3+} is reduced to Fe^{2+}. This reduction accelerates the formation of excess Fe^{2+} ions in the system so that the hopping rate of electrons in ferrites rises [55].

Ni substitution in Fe_3O_4 catalyst improved the resulting electrocatalytic activity of the pure material (η_{10} = 406 mV). The effect was also similar in the case of substitution by other elements, such as Co, Mn, Ce with η_{10} of 353, 372 and 310 mV, respectively [53,57–59]. The observed decrease of η_{10} is due to the decrease in the free-activation barrier of the OER [60]. These studies showed that overpotential decreased significantly with increasing replacement until the maximum of x = 0.5 (where x represents the stoichiometric factor in formula, for example $Mn_xFe_{3-x}O_4$). By increasing the Co content, the catalyst particle size decreased (increase in active area) and the formation of an amorphous structure was favoured [57]. The best substituents turned out to be: (i) Mn in combination with Ce ($Ce_xMnFe_{2-x}O_4$; x > 0.2), reaching the η_{10} of only 310 mV (1 M KOH, 25 °C) [55], due to the synergy between Mn^{2+} and Ce^{3+} centres in the cubic spinel lattice; and (ii) Ni in combination with Cr (η_{10} of only 228 mV), due to the above-mentioned synergistic effect between the two metal centres [61].

Inverse spinel oxides have the common formula $B[AB]O_4$, in which the divalent cation A occupies an octahedral site and the trivalent cations B occupy one octahedral and one tetrahedral site. In $NiFeMO_4$, the M^{3+} ions could occupy either the octahedral or tetrahedral site. Investigations are focused on partially replacing Fe by d-electron deficient metals, such as V [62], Cr [63–66] or Al [67]. The performance of $NiFeVO_4$ deteriorated by about 50 mV compared to Fe_3O_4 [62]. On the other hand, the performance of $NiFeCrO_4$ improved to about 160 mV compared to Fe_3O_4 (1 M KOH, 25 °C) [66]. However, the observed beneficial effect of Cr is not well understood. Nevertheless, it was observed that Cr-substitution mainly improved the electronic properties of the base oxide.

Besides oxides of the various transition metals, layered double hydroxides (LDH) of Ni and Fe seem to be very promising materials for the OER. These hydroxides represent a category of layered materials consisting of positively charged layers and charge-balancing anions in the interlayer region [68]. Their typical structure can be seen in Fig. 3a. Their performance can be improved by subsequent

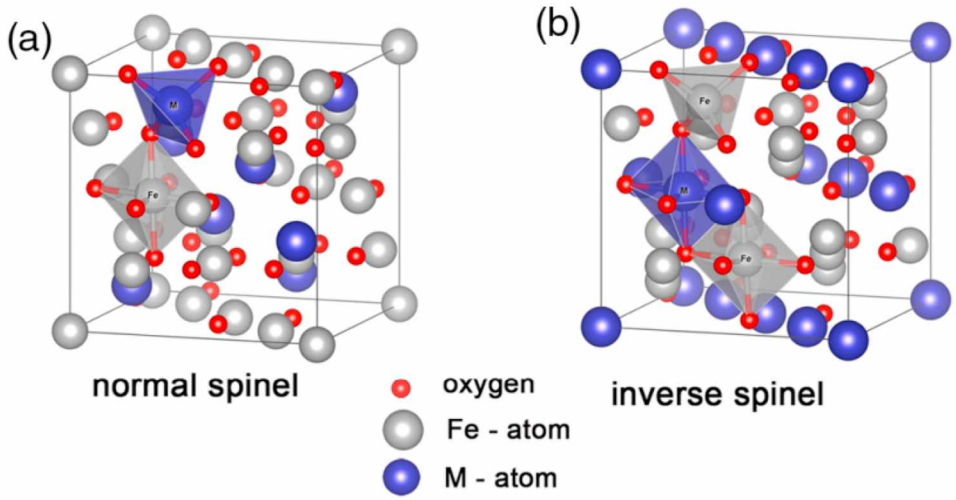

Fig. 2. Normal (a) and inverse (b) spinel structure of metal ferrite [56] (DOI 10.1117/1.JPE.7.012009).

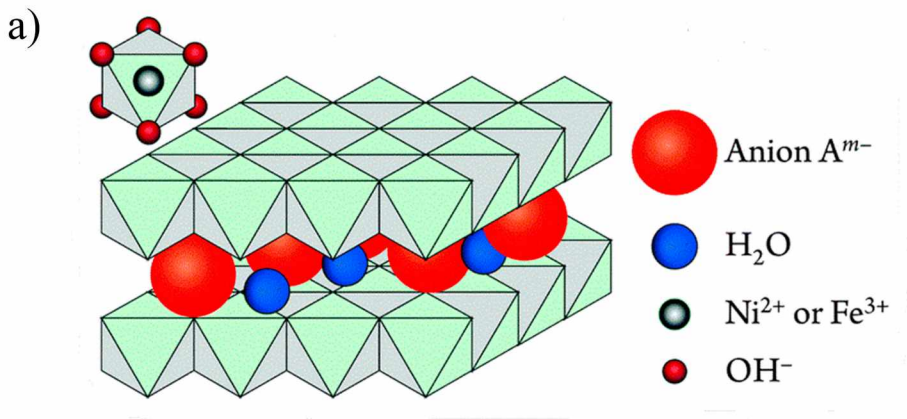

Fig. 3. a) Schematic illustration of the [NiFe]-LDH structure. Charge-balancing anions and water are present in the interlayer region, and Ni^{2+} or Fe^{3+} ions are surrounded by six hydroxides in distorted octahedral coordination (upper left). Reproduced from Ref. [71] with permission from the Royal Society of Chemistry and b) Preparation of LDH nanosheets by delamination in formamide under mechanical shaking (precipitation of LDH by AQS: anthraquinone-2-sulfonate anions, $C_{14}H_7O_5S^-$; anion-exchange into DS: dodecyl sulfate, $C_{12}H_{25}OSO_3^-$). Reproduced with permission from Ref. [72]. Copyright 2015 The American Chemistry Society.

delamination/exfoliation of LDH platelets into unilamellar nanosheets during preparation, as can be seen in Fig. 3b. This leads to the exposure of all transition metal atoms, which is favourable to acceleration of the OER due to rapid transport of the reactants to the reaction site [69]. The performance can be further improved by appropriate combination of the transition metals in the structure, for example in Co–Fe or Ni–Fe LDHs, the varying electronic structure of Fe sites (2+, 3+, 4+) and the synergy effect between Fe and M (= Co, Ni) can stabilize OER intermediates that are unfavourable on M-M centres [70].

Among many of the studied materials [68,69,73–75], hydrothermally grown Ni–Fe LDH with Pd nanoparticles showed the best activity with η_{10} as low as 156 mV (1 M KOH, 25 °C). The deposited Pd induces a higher oxidation state of Ni and Fe species, which is responsible for the improved OER activity.

Different preparation methods are used for Fe-based spinels, including co-precipitation [76]; pulsed-laser deposition (PLD) [77]; cathodic electrodeposition [78]; spin-coating [46]; aerosol spray method [79]; template synthesis [80]; or solid-state reaction [81]. PLD can ensure exact control of the amount of the deposited material, enhance adhesion due to the energetic nature of the procedure, and can yield a nanostructured material [77]. Of all these methods, the aerosol spray method is suitable for uninterrupted fabrication and optimization of amorphous metal oxides with changeable compositions and mesoporous structures. Active amorphous material (Fe–Ni–O_x) with overpotential η_{10} of only 286 mV and a Tafel slope of 48 mV dec^{-1} (evaluated at overpotential < 300 mV) was prepared by this method [79]. Beside

aerosol spray method, electrodeposition led to the preparation of amorphous mesoporous nickel–iron composite nanosheets with a three-dimensional structure, too [82].

Most of the catalysts mentioned previously perform well in an alkaline medium. However, the trend in research of alkaline water electrolysis technology today is to introduce an anion selective polymer separator, which has some advantages (e.g. ionic conductivity in the demineralised water environment, dense nonporous structure etc.) and allows the current KOH circulating electrolyte to be replaced by demineralised water. This is due to the higher safety and flexibility of technology operated with pure water. The activity and stability of the catalyst materials under neutral pH conditions thus represent an important advantage. For this reason, this point will also be discussed in the following chapters. Lowering the pH to near-neutral or neutral causes a decrease in hydroxide ion concentration; thus, their activity also decreases [83]. Moreover, under near-neutral pH conditions, protons are generated by surface reactions. Thus, protons must be removed from the surface to prevent corrosion of the electrode due to the local pH shift. In electroanalytical studies, this problem is usually solved by using phosphate buffer as the electrolyte instead of pure water. When the buffered species is present, the removal of protons from the surface is easier due to the chemical reaction between the buffering species and the surface protons [83,84]. In the case of Fe-based catalyst, Fe_3O_4 was also tested under neutral conditions [85,86]. A simple Fe-based film reached η_{10} of 630 mV (0.1 M phosphate buffer) with a low Tafel slope (47 mV dec^{-1}) [85]. For industrial conditions, however, demineralised water is preferred to phosphate buffer as a circulating medium as no chemicals need to be added and handled.

From all these studies it is clear that A or B substitution of Fe_3O_4 leads to a better performance of this spinel oxide catalyst. It was also shown that the best substituents are Mn, Ce or Cr. Moreover, even better results were shown when utilizing delaminated Ni–Fe layered double hydroxides, in which case η_{10} reached only 156 mV (1 M KOH, 25 °C). A Fe-based catalyst is also applicable in a neutral environment. However, overpotential is typically higher than in an alkaline one.

3.1.2. Co-based spinels

During the last five years, Co has attracted attention with regard to the OER application, due to the mixed valence states ($Co^{2+}/^{3+}/^{4+}$). The increased oxidation state of Co with a higher valence is believed to accelerate the multielectron transportation process involved in the oxidation of water [87]. Furthermore, it is generally accepted that the phase transformation of Co-based materials, such as oxides (Co_3O_4), to hydroxides or oxyhydroxides during the OER process, plays an important role. Moreover, the activity of Co oxide is also dependent on the surface area, morphology [39] and electronic states [88]. Based on this, researchers are focusing on developing new nanostructures with a large surface area [89] or different particle sizes [90] in order to improve OER performance.

The standard Co_3O_4 has a spinel structure, which consists of Co^{3+} at the octahedral sites and Co^{2+} at the tetrahedral sites. It is agreed that the surface of Co_3O_4 is partly oxidized to a CoOOH phase, and further to the CoO_2/CoOOH redox couple [91]. These results suggested that the presence of Co^{4+} may be crucial to catalyse the OER [19,92] as O–O bond formation is proposed to happen from the reaction of water with oxo Co^{4+}. Thus, with multiple oxo Co^{4+} sites, there will be a high possibility for two oxo Co^{4+} to become neighbours. As soon as a Co^{4+}(=O)–O–Co^{4+}=O site appears, a spontaneous water-dissociation process can happen [93]. The activity can be further increased by tuning the size and nanostructure of Co_3O_4 [94,95]. Superior catalytic performance can be achieved with Co_3O_4 nanoparticles with an average diameter of 5.9 nm (η_{10} = 328 mV; 1 M KOH, 25 °C) [90,91] compared with traditional bulk materials with a cubic structure and a high specific surface area [96–99]. They usually reach η_{10} of 450 mV (1 M KOH, 25 °C) [98].

A commonly used means of Co_3O_4 catalyst optimization is by doping on the A site. One of the possible dopants is Li, which can occupy either the octahedral or tetrahedral sites of the spinel lattice, depending on the method of doping [100]. The preferred site to be occupied is the tetrahedral one due to the Li^+ ions being small and easily moved [101]. Moreover, when Li is in the tetrahedral site, the charge compensation is accomplished by Co^{4+} ions in octahedral spinel sites [102]. The optimum amount of Li was found out to be 10 wt% [97,103–106] reaching a minimum η_{10} of 254 mV (15 wt% KOH, 60 °C) [97].

Besides lithium, Ni, Cu or La atoms are also mentioned in the literature as possible dopants as their substitution leads to a decrease in catalysts' electrical resistivity [102,107,108]. When Cu ($x > 0.2$) is used, a transition from a normal to an inverse spinel occurs [102], i.e. Cu^{2+} ions appear in the octahedral spinel sites. But this doping leads to an increase in η_{10} up to 629 mV (1 M KOH, 25 °C) [107,109,110]. Doping with La appeared to have no significant effect on the structure of the spinel phase, but it can decrease the resistance of the catalytic film as well as the charge transfer resistance and increase the metal/oxide roughness, delivering the η_{10} of only 267 mV (1 M KOH, 25 °C) [111]. Other strategies for improving the activity of the Co_3O_4 catalyst are usually coupled with other materials and the preparation of these coupled catalysts in the form of nanomaterials [112–116]. All these materials benefit from synergistic effects between two different phases, having rich oxygen vacancies, a high roughness factor, more active sites and favourable surfaces for the adsorption of oxygen-related species during water splitting [117].

Probably the most common choice of dopant element is Ni [118–122]. This is because nickel-cobalt oxide represents a reliable catalyst for the OER with high reproducibility and acceptable catalytic activity with η_{10} of 361 mV (1 M KOH, 25 °C) [123]. Because of its availability, different preparation methods of $NiCo_2O_4$ were studied, including coprecipitation of Ni – Co mixed oxalate [124], coprecipitation of Ni - Co mixed hydroxide [124], evaporation technique [124], freeze – drying technique [124], thermal decomposition [124], spray pyrolysis [125], propionic acid sol-gel method [126], microemulsion method and sol-gel method [127]. Both coprecipitation methods manifested improved activity and the hydroxide coprecipitation surpassed all the methods after ageing of the electrode, caused by an increase in active surface area. The thermal decomposition produced oxides with very good electrocatalytic properties, but, contrary to catalysts prepared by coprecipitation, their activity is lost after electrochemical ageing. Freeze drying led to the formation of a catalyst with different morphology, which also lost its electrocatalytic activity after ageing [124]. Spray pyrolysis led to the formation of a porous, uniform and crack-free morphology which did not change after 24 h of polarization. The calcination temperature was studied for the method of coprecipitation, and the optimum was set at 325 °C. This is important because insufficient temperature does not lead to the formation of the preferred spinel phase and a high temperature causes large sintering, causing a deterioration in the specific surface area of the electrocatalyst [127].

Regarding the use of catalysts in a near-neutral medium, selected Co based catalysts were also studied in buffered solutions. Pure Co_3O_4 can be used in the form of layered double hydroxide doped with Ni, Fe or Mn [128,129] or it can be coupled with carbon nanotubes [94]. Doping is also a strategy for performance improvement. The usual dopants are: Fe [130], Li [106], Ir [131], Ni [115], S [132], Cu [110] or Mn [110]. The lowest η_{10} was achieved using Co doped with Ir (373 mV, 1.0 M phosphate buffer solution, 25 °C). The improved activity is caused by the formation of Co oxyhydroxide and high valence Ir species with a low-coordination structure due to the high oxidation potentials, which together provide an outstanding OER performance [131].

3.2. Perovskites

Compared to spinels, a key advantage of perovskite oxides is flexibility in tuning their physico-chemical and catalytic properties. Their general formula is, as already mentioned, ABO_3 (see Fig. 4c for structure), where A sites correspond to rare earth or alkali metal ions and B

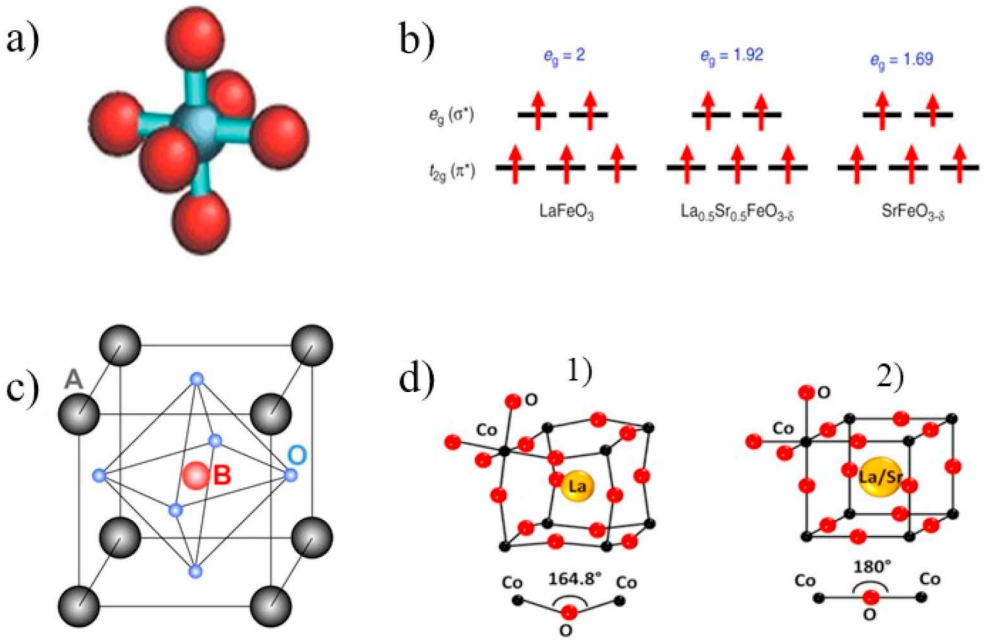

Fig. 4. a) Structure of octahedrally coordinated BO6 sites [143]; b) 3d electron occupancy of t_{2g} (π*) and e_g (σ*) antibonding orbitals associated with the transition metal, for $LaFeO_3$, $La_{0.5}Sr_{0.5}FeO_{3-\delta}$, and $SrFeO_{3-\delta}$ [136]; c) ABO_3 structure of perovskite [143] and d) Evolution of the pseudocubic (1) and cubic (2) cell parameter as a function of the Sr doping. Reprinted with permission from Ref. [135]. Copyright 2015 American Chemical Society.

sites to transition metal ions. In an ideal unit cell, the A-site cations are usually more electropositive and larger with 12-fold coordinated oxygen, whilst B-site cations are more electronegative and smaller with 6-fold coordinated oxygen. Due to the high adaptability of their electronic composition and the choice of metal cations, resistance to corrosion in alkaline media, moderate cost and low environmental hazard [133], improved perovskites have been gradually developed and modified [134]. Moreover, it was shown that their catalytic activity can be further influenced by substitution or partial substitution of the A- and/or B-site by other elements, resulting in $(A_xA'_{1-x})$ $(B_yB'_{1-y})O_3$ structure [135]. B is typically metal with the electron configuration 3d, 4d or 5d. In an octahedral coordination, the d orbitals can be divided into two groups: three t_{2g} (π*) orbitals, that have a lower overlap with the neighbouring 2p orbitals of the oxygen ions [117], and the e_g (σ*) antibonding orbitals that are headed towards the oxygen atoms [136]. Better catalytic activity for the OER can be achieved by using B-site transition metals which have an e_g occupancy close to unity [137].

In the low overpotential region the rate-determining steps in the OER on perovskites are Reactions 2 or 3, depending on the material [138]. But, at high overpotential ($\eta > 400$ mV) it seems that the decomposition of the OOH intermediate to O_2 represents the rate-determining step [139]. The transition metal cations with e_g occupancy close to unity facilitate these two RDS effectively and lead to the highest OER activity [140]. Moreover, by selecting an ABO_3 perovskite, the charge transfer is improved due to covalence among the metal 3d orbital and oxygen 2p orbitals in the transition metal–oxygen complex at the B-site [141]. The OER activity of perovskite oxides would be further enhanced by widening the σ* (antibonding) band [135]. An extended σ* band should improve the electron shift between the OH^- and the oxide catalyst surface. OER performance is also improved by introducing oxygen vacancies [142]. It was shown that, by tuning the electronic structure of perovskites, such as reducing the oxygen vacancy content and shifting the Fermi level of oxides closer to the oxygen 2p-band centre via substitution of divalent ions on the A-site, the OER activity can be greatly increased. On the other hand, if the O 2p-band is too close to the Fermi level, it can cause A-site cation leaching and amorphization of the surface [142].

The OER active site for perovskite oxides lies in the octahedral coordinated BO6 sites (Fig. 4a), which contain the B-site transition metal cation and the oxygen anion. B-site cations have a critical compositional effect on the OER mechanism and stability. For example, the possible positions for the adsorbates on a Co–O terminated surface were studied and it was found, that the most suitable electronic states for formation of the bonds are the oxygen valence states (p electrons) and metal valence states (d electrons). Hybridization of the metal d orbitals and oxygen 2p orbitals can occur due to the overlap and energetic resemblance of the electronic states. The overlap of d and 2p orbitals results in the formation of σ-bonding and σ*-antibonding states [144]. Hence, the most energetically favourable position is along the nearly linear O–Co–O bridges [133].

Of the transition metal-based perovskite oxides (such as Mn, Fe, Co and Ni), Co-based oxides have emerged as promising candidates owing to the outstanding OER performance of the CoO6 octahedron. Co in a perovskite structure usually has more oxidation states (Co^{2+}, Co^{3+} and Co^{4+}) and spin states than Ni (Ni^{2+}) and Fe (Fe^{3+}). The formation of higher oxidation states of Fe requires high pressures during the synthesis. For example, Fe^{4+} oxides are synthesized under the pressure of several GPa [145]). A higher oxidation state of Ni is reached by oxidizing β-$Ni(OH)_2$ using a 0.5 mol dm^{-3} $K_2S_2O_8$ as an oxidant in 6 mol dm^{-3} KOH solution at 80 °C for 60 min [146]. Co^{3+} and Co^{4+} cations are helpful in the formation of MOH and MOOH, respectively, under alkaline conditions [147]. According to DFT calculations, $SrCoO_3$ and $LaCoO_3$ are located on and below the top of a volcano plot for the OER activity [148]. Thus, they should represent the most active catalysts of the perovskite group. Cubic $SrCoO_3$ is expected to provide the highest OER activity as its large σ* bandwidth causes an increase in the rate of electron transfer [138]. One problem is the preparation of an ideal perovskite cubic structure. Typically, incompletely oxidized $SrCoO_{3-\delta}$ is prepared, which has a hexagonal phase structure [135]. It was suggested that the overlap between Co cations and O^{2-} ions in the lattice of $SrCoO_{3-\delta}$ might decrease on account of the non-aligning of Co–O–Co and the high amount of oxygen vacancies, thus degrading its conductivity

and OER activity [149].

Perovskites can be doped in many ways. As mentioned above, usually A-type or B-type substitution is studied. Typical A-site elements are La, Sr, Ca [135,147,150–153], but elements such Sc, Ba, Pr, Sm, Nb, Gd, Ho and Y are reported, too [133,152,154,155]. B-type substituents are typically represented by Co, Ni, Fe, Cr, Mn, Ti, Sc, Sr and Mo [142,156–166]. Another possibility is anion doping, such as $SrCoO_{2.85-\delta}F_{0.15}$ [167].

When Sr is used as a dopant, a typical η_{10} of these materials reached 400 mV [142,147,151,153,161,164,165,167,168], which agrees with the above-mentioned improved performance of $SrCoO_3$. Substitution of Sr does not cause amorphization of the samples because of lower O p-band centres relating to the Fermi level [150]. Amorphization was observed to occur, for example for $Ba_{0.5}Sr_{0.5}Co_{0.4}Fe_{0.6}O_{3-\delta}$, by leaching of Ba^{2+} and Sr^{2+} ions from the surface [150]. Doping with Sr also led to a less adherent and cracked structure, and consequently the roughness factor increased [151]. Moreover, Sr substitution caused a change in the structure of $LaCoO_3$ from pseudocubic to cubic, as can be seen in Fig. 4d. This resulted in an increase in conductivity, probably because of the substitution of La^{3+} by the larger Sr^{2+} cations, which led to the alignment of the Co–O–Co bonds (straightening of the octahedral cage) and the further oxidation of Co (beyond Co^{3+}) [135].

Besides Co, using Ni as the B-site cation has been proven to be beneficial [169,170] because it leads to the formation of a cubic structure of the catalyst, too. On the other hand, when Ti was used as the B-site cation, the η_{10} reached for resulting $SrCo_{0.9}Ti_{0.1}O_{3-\delta}$ the value of 510 mV (0.1 M KOH, 25 °C). This is a higher value when compared to the original $Ba_{0.5}Sr_{0.5}Co_{0.8}Fe_{0.2}O_{3-\delta}$ sample with $\eta_{10} = 400$ mV. It indicates that doping with Ti is ineffective, as the redox reaction of Ti^{4+}/Ti^{3+} is unfavourable under these operation conditions [158,171]. When Ba^{2+} together with Sr^{2+} ions is used, leaching was observed [150].

Different preparation methods for Ni-based perovskite were also studied. The catalyst was synthesized by the hydroxide solid solution precursor method [172], hydroxide coprecipitation method [172], propionic acid sol – gel method and malic acid method [126]. The best one turned out to be the malic acid method, due to which it was possible to prepare the catalyst at a lower temperature (600 °C) compared to other options (approx. 800 °C) [126]. The perovskite with cubic structure ($SrCoO_3$) was prepared by electrochemical and chemical oxidation of the defective orthorhombic $SrCoO_{2.5}$ [173]. Otherwise, the cubic structure is usually obtained by doping [167].

Some types of perovskites were also studied for their possible use in water electrolysis under neutral pH conditions (e.g. $LaCoO_3$, $LaNiO_3$, $LaMnO_3$ and $LaFeO_3$) [148]. Perovskites with O p-band close to Fermi level demonstrated leaching of A-site atoms and amorphization of the surface under all overpotentials. Those with O p-band far from the Fermi level were stable under low OER potential but became unstable at high OER potential and leaching of B-site atoms was observed. For example, the overpotential of $LaNiO_3$ was 220 mV (at 5 μA cm^{-2}) and it was able to achieve a stable current density of 18 μA cm^{-2} at 1.83 V after 2 h [148]. At the current density of 50 μA cm^{-2}, the Sr_2GaCoO_5 required an η of 300 mV. The current density at 1.65 V vs RHE was measured as 1.7 mA cm^{-2} for 5 h [174]. However, these current density values fall short of the demands of industry.

Considering all the oxide materials mentioned in this chapter, it is possible to conclude that much effort has been dedicated to preparing active catalysts with various compositions and structures. Regarding perovskite oxides, electronic structures (e_g electron, d-band centre, and O p-band centre) are the major optimization approach for design of the catalyst. In addition, lattice oxygen activity and surface modification also provide new insights into the OER under real conditions [15]. Another attempt is to increase the number of active sites on the surface or, to improve the catalysts' intrinsic activity by an active control of the active site. The future of these materials consists in optimization of the catalysts' surface by employing nanostructures, porous materials or by controlling their morphology [81]. However, the drawback of metal oxide electrocatalysts is usually their poor electroconductivity.

Both spinels and perovskites were studied under near-neutral pH conditions. Considering spinels, pure Co_3O_4 seems to be applicable, as well as Co_3O_4 doped with other elements (e.g. Fe, Li, Ni, Cu). On the other hand, perovskites showed very low current densities in the order of μA cm^{-2} and as such are not very suitable for use in near-neutral media.

4. Phosphides

Besides transition metal cations, anions can also affect OER catalytic activity by modifying the covalency of the metal–ligand bond leading to modification of the redox potential of the catalytically active centre [175]. Many studies have suggested that transition metal phosphides (TMPs) could be ideal catalysts due to their low cost, abundance, high efficiency and extraordinary electrochemical properties [176–180]. TMPs have demonstrated good catalytic performance in many fields. For example, in the HER, TMPs have proven to be high-performance materials with superior activity, stability, and close to 100% faradaic efficiency in the full range of electrolyte pH [181]. Recent studies have shown that incorporating metal atoms, such as Ni, Co or Fe, into the lattices of TMPs allows further adjustment of the atomic coordination and electronic structure, resulting in improved catalytic activities. Phosphides with catalytic properties are mainly cobalt Co_2P [182,183], Ni_2P [184,185], FeP [186], and their mixtures [178,186–192].

Phosphides are frequently doped with Ni [121,188–193]. The performance of this combination is even further improved if the Ni_2P is doped with Fe [189,191,192,194]. For example, Ni_2P and Fe-doped Ni_2P nanoparticles reached η_{10} of 246 and 205 mV (1 M KOH, 25 °C), respectively. Both the η_{10} values and the Tafel slopes decreased with increasing Fe doping due to the change in electronic structure related to the bimetallic alloying. The stability of the catalyst was tested galvanostatically for 22 h at a low current density (10 mA cm^{-2}) in 1 M KOH at 25 °C. Only a negligible change in the properties was observed. When the current density was increased (300 mA cm^{-2}), an increase in potential of approx. 38 mV was observed over the 22 h. During the potentiostatic test, the current density decreased by only 4 mA cm^{-2} (from an initial value of 156 mA cm^{-2}, 1 M KOH, 25 °C) over 110 h of electrolysis at a cell voltage of 1.6 V [190]. It was observed that the original nanotube structure disappeared, being replaced by numerous flock sheet structures scattered in an amorphous matrix. Furthermore, no metallic Ni and Fe states were detected on the surface of the catalyst. On the other hand, the oxidation of phosphide to phosphate was observed [190]. Ni_2P and Fe-doped Ni_2P catalyst were analysed post-OER. It was discovered that, in the process of the OER, the metal oxides/hydroxides are formed in situ and replace the initial phosphides as the new catalytically active sites. Considering the Ni_2P core, it might be the ideal template to grow these specific oxides (e.g. NiO_x), and synergistic effects might exist between the phosphide core and the oxide. This theory, however, requires further study for confirmation [185]. Moreover, with an increase in Fe content, more Fe active sites are generated on the surface, whereby the catalytic performance is enhanced [195]. Hence, the true catalytically active site is probably not the metal phosphide but its oxidized products and, as such, metal phosphides more likely act as "pre-electrocatalysts" [179].

Another possible dopant is cobalt with η_{10} being usually around 345 mV [183,186,187,191,196,197]. However, when Cu is used as the dopant (the only element, or jointly with Co), the performance is even worse [198]. Pure Cu_3P shows a bulk structure, which may be the reason for the inferior performance ($\eta_{10} = 419$ mV; 1 M KOH, 25 °C). However, more interestingly, when Cu_3P is coupled with Ni_2P, nanosheets are formed, leading to a significantly improved performance ($\eta_{10} = 262$ mV), which is explained by the synergistic effects between the two materials [121].

Other doping strategies were studied such as coupling of Co/Co_2P [196]. This mesoporous catalyst reached η_{10} (1 M KOH, 25 °C) of only

57 mV, which is much better compared to RuO_2 as well as other types of catalysts discussed in this review. This catalyst was obtained by hard-templating, i.e. by a method suitable for the synthesis of porous structures with a 3D network, high porosity, and excellent structural strength. The synthesis involved reductive thermal treatment of dichlorobis(triphenylphosphine)cobalt(II) ($(PPh_3)_2CoCl_2$) in a N_2 atmosphere containing 10% H_2 using a silica template [199]. The resulting pore diameter of this material was 4.5 nm and the surface area was 292 $m^2\ g^{-1}$. The stability was tested at 10 mA cm^{-2}, and the cell achieved a potential of 1.61 V vs. RHE, which remained stable for 24 h [196]. However, the stability test needs to be verified under the harsher conditions of industrial water electrolysis. Beside the high specific surface area, which is about 4 times higher than for Co_2P catalyst, the presence of metallic cobalt increases the electron conductivity of the catalyst. Both aspects impact positively catalytic activity of the resulting material.

Not only cations can be partially substituted, but also anions. For example O–Ni_2P [192], Ni–Fe–P–B [191], Co–Fe–P–S [186] or Co–P–B [200,201] were studied, but all these materials showed an average value of overpotential. In the case of Co–P–B, its advantage is its electron transfer mechanism, which combines the advantages of electron loss between Co and B and electron gain between Co and P.

Besides the hard-templating, metal phosphides can be prepared by chemical vapour deposition [202], electrochemical dealloying [195], or electrodeposition [203]. Through chemical vapour deposition it was possible to prepare nanocrystalline Fe–Ni–P with η_{10} of only 154 mV (1 M KOH, 25 °C), with FeP and Ni_2P particles with diameters of 5–30 nm. Under AWE conditions, the cell voltage to afford a current density of 10 mA cm^{-2} was only 1.42 V (1 M KOH, 25 °C) [202].

Phosphides were also studied under OER conditions in a neutral pH environment. The usual composition of catalysts tested was Co–P [204–211], which reached a η_{10} of about 430 mV (0.1 M phosphate buffer). Besides Co, a combination of Ni and Fe is used (Ni–Fe–P) [212,213] with η_{10} of 396 mV (0.1 M phosphate buffer). A significant drawback of this material is its stability, which is low due to continuous dissolution of Ni/Fe into the neutral electrolyte [213].

In summary, in phosphide-based materials, both cation and anion substituents are able to improve the catalytic activity and stability of the resulting catalyst if the electronic structures of the base materials are modified. The role of cations and anions is important in optimising the electrocatalytic activity because they can significantly increase the number of active sites in the electrocatalyst. Moreover, the improved OER performance can be ascribed to the synergistic effect between two or more cations. The post-OER study showed that phosphides tend to play the role of "pre-electrocatalysts", whose oxidation leads to the creation of the oxides/hydroxides, which are the true active sites.

The future of these catalysts consists in the preparation of a bifunctional electrocatalyst, as phosphides are also widely used as a HER catalyst. The reason for lowering the overpotential lies in the formation of nanowire-like self-supported bifunctional catalysts with a porous structure, which can provide enhanced electroactive sites and facilitate the gas evolution.

5. Selenides

Transition metal chalcogenides have been extensively used for several applications, including high-temperature superconductors and photovoltaics. They have also been used for heterogeneous catalysis for oxidative ring expansion of methylenecyclopropanes to cyclobutanones using H_2O_2 as the oxidant. Recently, selenides were studied as HER catalysts. Due to their bifunctionality, they represent another interesting group of materials suitable for the OER. The structural richness of selenides along with enhanced electronic properties are highly favourable for further tuning of the electrocatalyst performance. Additionally, the promising OER electrocatalytic activities of Ni, Co, Fe or Cu-based selenides can be further enhanced [214]. Selenides are believed to have improved both the OER performance and the catalytic activity than oxides, due to the lower electronegativity of Se (2.55) compared to elemental O (3.44) [215]. This leads to increased covalency in the metal–chalcogenide bond, accelerating catalyst activation and the onset of the OER reaction by reducing the redox potential of the catalytic site [175].

The average η_{10} for different selenides with either Co, Ni or Fe cation has a value of around 300 mV [87,214,216–224]. Further doping with an additional element led to an increase in catalytic activity. For example, doping CoSe with Fe, Cu, Ni or P [87,219,221,225–232] proved to be beneficial. Regarding Co–Fe–Se, its improved activity is due to Co and Fe being in octahedral coordination, which demonstrates better catalytic activity than tetrahedral coordination. Cu, on the other hand, shows better activity in tetrahedral coordination [227]. Moreover, selenized Cu_3Sn@Cu foam was studied as a catalyst suitable for weakly alkaline pH (8.5) with η_{10} of 624 mV (1 M $NaHCO_3$) [232]. Concerning doping with Ni, Ni–Fe–Se, nanowrinkles with a 3D porous structure and abundant mesoporous structures reached the lowest η_{10} value of only 135 mV (1 M KOH, 25 °C). After 50 h of stability testing at 10 mA cm^{-2}, the OER overpotential increased only by 10 mV [233].

Selenides, as well as phosphides, act as "pre-catalyst" in the OER under alkaline conditions. It was found out that at the surface of the catalyst, part of Ni from NiSe transforms to NiOOH, which is the real-time OER catalyst [229]. NiSe forms the core of the catalyst, which accelerates the electron transport between the active layer and the electrode substrate. When doped with Fe or Co, the structure of $Ni_xM_{1-x}OOH$ (where M = Fe, Co or other metal) appears, enhancing the activity even more. This agrees with the fact that Ni–Fe–Se nanostructured material showed one of the lowest overpotentials [234].

Three preparation methods, including direct electrodeposition, a hydrothermal method and chemical vapour deposition (CVD), were mainly studied [87,235–237]. The structure of the electrodeposited film was uniform and composed of well-dispersed, randomly oriented nanoparticles. A very rough surface with high porosity was observed, which is advantageous for catalytic activity. Moreover, the nanoparticles together with mesopores enhance the specific surface area. The CVD and hydrothermally synthesized selenide showed a mainly granular structure. Moreover, electrodeposition and CVD methods allow the preparation of the catalyst without any binder, which is advantageous due to direct electrical contact with the electrode and elimination of non-active components, thereby maximizing charge transport and catalytic efficiency.

Nanostructured selenides (nanowire arrays, nanowrinkles) have drawn considerable attention due to their notable electrocatalytic activity. The most stable nanostructured catalysts that have recently been reported are prepared by either electrochemical deposition or hydrothermal/solvothermal growth of nanostructured catalysts on the desired substrate materials. The activity of these selenides can be further improved by doping with more than one element.

6. Other materials

In this chapter, different materials, not yet systematically and exhaustively studied, will be briefly introduced. The first group is represented by metal alloys. The mechanical alloying procedure is a good method for mixing a large range of elements in order to study their synergistic effects. The nature of the physical mixture, however, leads to large size crystals with a low electrochemically active surface area and shortage of chemical contact between the different elements [68,238]. This problem is eliminated when the alloys are prepared by electrodeposition on an appropriate substrate. The average overpotential of metal alloys prepared by electrodeposition is 374 mV [239]. Taking Ni as the most active material for the OER from the transition metals, it can be alloyed with Fe, where the optimal OER efficiency is achieved with 55 at.% of Fe [240,241]. Another element to create an alloy with Ni is Co. This alloy is more active than monometallic catalysts due to stabilization

of the active β-NiOOH phase by the addition of Co [242]. Ni–Co alloy can be further modified with Cr, Mn, Fe and/or Cu [239,243] with a significant increase in catalytic effectiveness for the Mn- and Cr-doped electrodes. Cr, Mn and Cu exhibit higher enthalpy of OH^- adsorption for the OER compared with Ni. In fact, the proper combination of d8-orbitals of Ni with d5-orbitals of Mn or d3-orbitals of Cr and d7-orbitals of Co boosts the catalytic activity of the electrode towards the creation of O_2 [244]. Sn can also be used as a dopant despite the fact that its overpotential is far behind the average value (473 mV) [245]. The reason lies in the observed excellent stability of this catalyst, which was subjected to an accelerated service life test corresponding to 5 years of operation [246,247].

Besides the alloys with a relatively simple structure, an alloy composed of Bi_2Te_3@CoNiMo was also studied [248], where CoNiMo alloy was formed as nanoparticles (NPs). In this case, the alloy was prepared by solvothermal method. The synergistic effects between Bi_2Te_3 and CoNiMo, as well as an increased amount of Co, can significantly improve the catalytic activity, as seen from the low η_{10} of 80 mV (0.9 M KOH, 25 °C).

A further group of materials used is represented by carbon. Pristine carbon can be utilized, for example, in the form of nanotubes [249] with a diameter of 2–5 nm and η_{10} of 450 mV. These pristine nanotubes (CNTs) can be further used as a substrate modified by other catalytically active material like Ni–Fe layered double hydroxide (NiFe-LDH) [250] or Co_3O_4 [251]. Here, the high electrocatalytic performance is attributed to the strong link between the catalyst and the CNTs, which facilitated charge transport. Other form of carbon used for catalysis is graphite foam modified with Ni-doped α-FeOOH (Ni:FeOOH) nanosheets [252]. Carbon nanofibers can also be modified with Co and Fe nanoparticles [253]. The carbon layers protected the catalyst particles from detachment or dissolution from the support. More efficient for catalysis is N-doped carbon.

The N doping makes no difference to the morphology and nanostructure of the samples but it greatly increases their electrochemically active area [14]. One of the best performances was reached with Co-embedded N-rich carbon nanotubes (η_{10} only 150 mV in 1 M KOH, 25 °C) [254–258]. Despite the good performance of carbon-based catalysts, there is a potential problem with their stability. As can be seen from Fig. 5, at high pH (alkaline), carbon is not stable in the potential range needed for water electrolysis [259]. This problem was studied by Wang et al. [260], who considered carbon oxidation under OER conditions in an alkaline environment. High-surface-area carbon black was used as a model material with η_{10} of 430 mV. However, after the first scan of the OER test at 2 mA cm^{-2}, overpotential increased significantly. The cause of this large deterioration of the oxidation current may be because the carbon black has undergone severe oxidation during the potential scan, which leads to an increase in the charge transfer and transport resistances. Moreover, the amount of surface oxygen content increased significantly after the OER test (from 2.86% to 41.8%). Thus, the stability of carbon-based materials under OER conditions should be considered, especially for the long term [260].

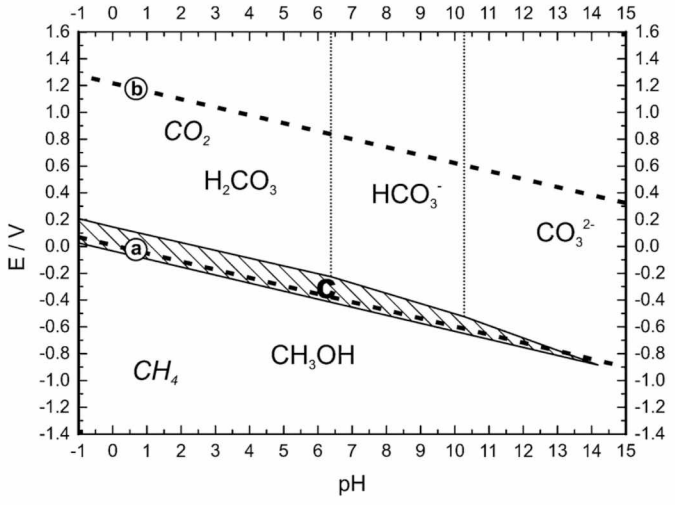

Fig. 5. Pourbaix diagram for carbon; dashed lines corresponding to stability of water. Reproduced from Ref. [259] with permission from The Royal Society of Chemistry.

For catalysis purposes, stainless steel activated over time was studied [261]. The activation was performed by a very slow and spontaneous change in the surface composition under the long-term OER in concentrated LiOH. Under these conditions, an active passivation layer with a high amount of Ni is obtained. The stainless steel can further be coated with a Co–Ni layer [262]. Other materials are: amorphous MnO_2 [263], IrW nanobranches [264], which were also tested under near-neutral pH conditions (1 M phosphate buffer), RuO_2 impregnated with CeO_2 [265] or hollow $CuS_{0.55}$ nanoparticles on a Cu foam [266]. Besides IrW nanobranches, Ni and Co borates were studied under neutral conditions (0.1 M potassium borate) [267,268] as well as ZrS_3 in the form of ultrathin nanosheets (mixed phosphate buffer solution (pH = 6.9)) [269].

Metal alloys seem to be a promising catalytic material thanks to a synergistic effect among the different nanomaterials, such as Bi_2Te_3@-CoNiMo. Carbon was also studied for its interesting catalytic activity, which, in the case of carbon nanotubes or nanofibers, is sufficient and can be improved by the addition of nitrogen. However, the problem of carbon concerns its long-term stability under OER conditions.

7. Comparison of different materials

In this section, different catalyst materials are compared. Aspects of comparison of catalytic activity of the materials published by different authors has been into the detail discussed in Ref. [270]. Main issue represents absence of unified, generally accepted testing protocol allowing direct comparison of the data reported. On the base of extensive literature analysis, following parameters were proposed as comparison criteria: (i) overpotential at a fixed current density, preferably 10 mA cm^{-2}, (ii) Tafel slope and (iii) catalyst loading at which the test was performed. An important aspect represents also stability of the catalyst. Although the stability tests reported in the literature are typically performed for tens of hours [271,272], duration of hundreds of hours would be more conclusive, as the technology should operate for several years [246]. Based on this analysis, the η_{10} (overpotential at current density of 10 mA cm^{-2}, 1 M KOH, 25 °C) was used as a main parameter distinguishing between different catalysts reported. The comparison is made according to the box graphs presented below. Different values can be observed in the graph. The numbers refer to: 1) outlier points (above 90th percentile); 2) 90th percentile); 3) 75th percentile; 4) mean; 5) median; 6) 25th percentile; 7) 10th percentile; 8) outlier points (below 10th percentile). All the materials together with the values of η_{10} used to create the graphs are summarized in Table S1 in Supporting Information.

In Fig. 6 the overpotentials are compared between RuO_2 and single-metal oxides, phosphides or selenides of Fe or Co. Ni has been used as an undoped and state-of-the-art electrocatalyst in the form of NiO or Raney-Ni for decades, but for last years it is much more often used as a dopant and as such is not included as a single-metal catalyst in this review, but it is mentioned later as a dopant for Co or Fe-based catalysts. The mean value of η_{10} for noble catalyst is 344 mV (pH 13–14, temperature 25 °C). The lowest η_{10} was reached with RuO_2 doped with Ir (124 mV) [273]. The mean value of η_{10} for Fe is 493 mV. The lowest η_{10} (438 mV) was measured for Fe_3O_4 prepared by the hydroxide precipitation method [60], the highest was measured for Fe_2O_3 nanoparticles (550 mV) [53]. Co, on the other hand, has a mean η_{10} of 383 mV, which is only 39 mV higher than RuO_2. The lowest value of overpotential was reached when $CoSe_2$ was used (around 290 mV) [220]. On the other hand, the highest

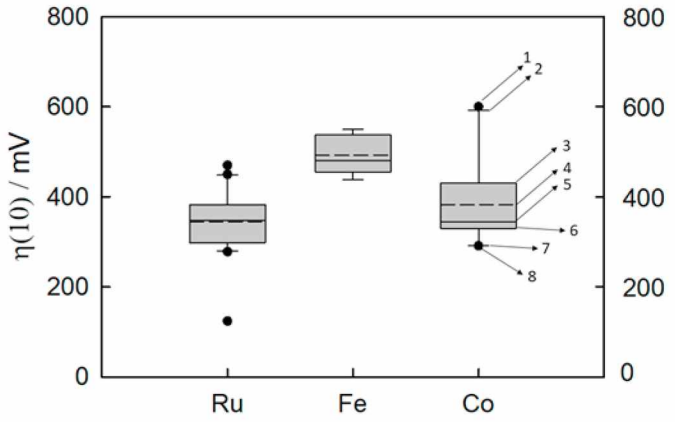

Fig. 6. Value of OER overpotential at 10 mA cm^{-2} for pH 13–14 and temperature 25 °C for single-metal oxide catalyst, phosphide or selenide compared to noble RuO_2; 1) outlier points (above 90th percentile); 2) 90th percentile); 3) 75th percentile; 4) mean; 5) median; 6) 25th percentile; 7) 10th percentile; 8) outlier points (below 10th percentile). Catalyst load is not considered.

overpotential (600 mV) was observed for Co_3O_4 [152].

As can be seen in Fig. 7, the effect of doping Co- and Fe-based materials with other metals on OER overpotential was studied as well. The average η_{10} for Fe-based materials was 354 mV, which is 139 mV lower than that of the undoped Fe catalyst. Considering the lowest obtained η_{10}, the overpotential decreased by 303 mV. On the other hand, the average overpotentials of doped Co catalysts was 360 mV, which is only 21 mV lower than that of the undoped catalyst. Nevertheless, the difference between the lowest overpotentials of the doped and undoped catalyst was 234 mV.

It is presumed that, in the case of Co-doped Fe oxyhydroxide, the Fe sites are the primary catalytic active ones, while the Co oxide serves as an electrically conductive host [274] with conductivity getting up to 1 S cm^{-1} (Pt substrate, sol–gel method from Co(II) sulfate precursor using a dip-coating technique, temperature 500 °C) [103].

Other researchers have argued that the presence of Fe stabilizes the higher oxidation levels of Co ions in binary Co–Fe oxides, thereby probably changing the rate-determining step of the reaction. Pure Fe_3O_4 is known to exhibit inferior catalytic activity toward the OER, and the oxidation of Fe^{3+} to Fe^{4+} has not been detected even when a large overpotential was employed. However, when doped with Co, Fe oxidation during the first reaction step only required a reaction free energy of 1.08 eV compared to the original value of 3.68 eV [275], suggesting that the Co oxide is able to stabilize the higher valence state of Fe (Fe^{4+}).

The effects of Ni and Mn doping on the overpotential of cobalt-based catalyst were modest [276]. In other work [277], it was concluded that the success of doping NiOOH with Fe derives from the ability of Fe to simply change oxidation states, which is critical during the OER. Specifically, similar free energy is needed for the transition of Fe^{3+} to Fe^{4+} and back. In contrast, pure NiOOH requires a large free energy for the transition of Ni^{3+} to Ni^{4+}.

In Fig. 8, a comparison of catalysts based on their anion nature is depicted. Oxides are the most studied materials, with an average η_{10} of 415 mV. Considering the values lower than 283 mV (10th percentile), it can be observed that many of these materials are Ni–Fe layered double hydroxides [68,69,73–75]. These materials contain metallic cations from the transition group and hence go through oxidation (M^{2+}/M^{3+}) in the range of the applied potential. This presence of transition metals in the layers has been suggested to enhance the charge transport of the material [278]. Moreover, the electrocatalytic activities of catalysts depend on their structures and electrochemically active surface areas. Ni–Fe LDH has a layered structure, and its interlayer space can be expanded by introducing anions and molecules of water between their neighbouring plates, providing hydroxide ions enough space to approach the active metal ions. However, Ni–Fe LDH catalysts are insulators and tend to aggregate into large particles. Therefore, carbon materials (e.g. carbon black, nanotubes and graphene) are frequently added to Ni–Fe LDH catalysts to improve their conductivities and prevent particle aggregation [279]. Palkovits et al. [280] compared about 6000 different catalyst materials in total with varying compositions $(Ni–Fe–Co–Ce)O_x$ and found out that in most cases the smallest value of η_{10} was around 350 mV. The average overpotential values ranged from 400 to 450 mV and the highest values were about 500 mV. These values correspond very well with our findings regarding the oxide materials. But materials with η_{10} lower than 350 mV were also found, suggesting there is a possibility of overpotential reduction.

Both phosphides and selenides are able to attain a lower average value of η_{10} (304 and 297 mV, respectively) than oxides. Compared with RuO_2, even the highest η_{10} obtained for FeP (480 mV) [197] is comparable with the highest η_{10} for RuO_2 (470 mV) [223]. The lowest overpotential (57 mV) was obtained for Co/Co_2P [196], which could be attributed to the higher surface area (292 $m^2\ g^{-1}$), the higher content of active sites, and the presence of metallic cobalt as a conductive

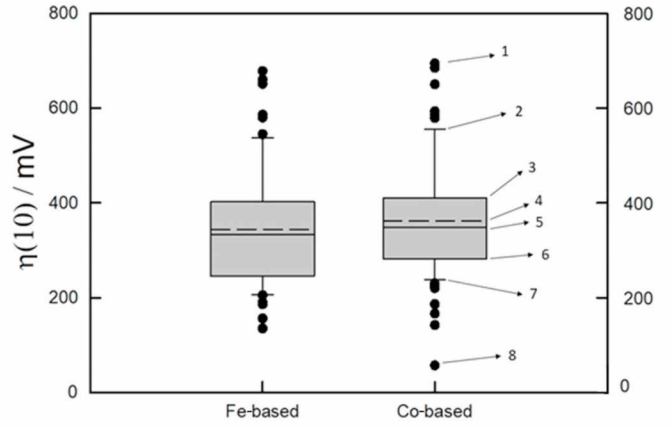

Fig. 7. Value of OER overpotential at 10 mA cm^{-2}, pH 13–14 and temperature 25 °C for Fe/Co-based oxide/phosphide/selenide catalyst doped with other elements; 1) outlier points (above 90th percentile); 2) 90th percentile); 3) 75th percentile; 4) mean; 5) median; 6) 25th percentile; 7) 10th percentile; 8) outlier points (below 10th percentile). Catalyst load is not considered.

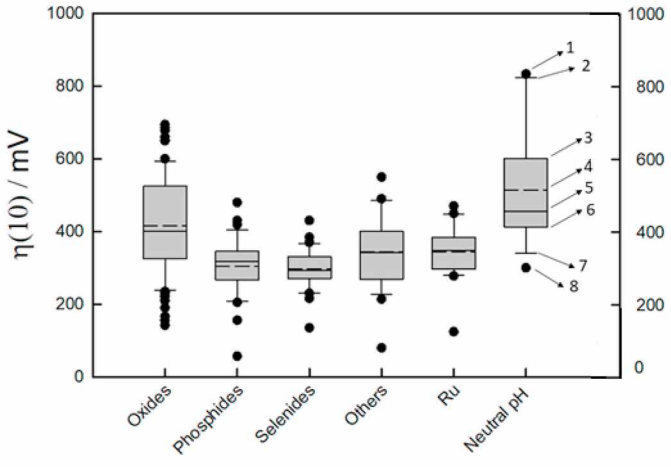

Fig. 8. Value of OER overpotential at 10 mA cm^{-2}, pH 13–14 and temperature 25 °C for oxides, phosphides, selenides and other materials compared with noble RuO_2 and to catalysts at neutral pH (6.4–9.2); 1) outlier points (above 90th percentile); 2) 90th percentile); 3) 75th percentile; 4) mean; 5) median; 6) 25th percentile; 7) 10th percentile; 8) outlier points (below 10th percentile). Catalyst load is not considered.

electrocatalytic material. This mesoporous catalyst (pores with a diameter of 4.5 nm) was prepared using a silica template. Furthermore, a low Tafel slope of 57 mV dec^{-1} was measured, indicating that the rate-determining step is a step subsequent to the first electron transfer reaction. However, the catalyst stability was only tested for 11 h (1 M KOH, 1.287 V vs. RHE, potential scan rate of 50 mV s^{-1}, starting current density of 10 mA cm^{-2}) [196]. Thus, this parameter will have to be properly verified. Considering the selenides, usually Ni–Fe–Se reached the lowest overpotential and good long-term stability for over 80 h (1.0 M KOH, 10 mA cm^{-2}, $NiSe_2$/Ni as the anode and cathode) [221,230,231]. The group marked as "others" contains material, such as carbon, stainless steel, MnO_2 and metal alloys. In this group, the best results were achieved with N-doped carbon, further coated with Ni, Fe or Co. The improved performance is possible to ascribe to the high conductivity of carbon, the synergistic effect of the metallic particles and the introduction of electron-rich nitrogen [256]. However, as mentioned earlier, the long-term stability of carbon-based materials under anodic oxygen evolution is unclear up to now.

Another important aspect for catalyst utilization on a large scale is its performance under neutral or near-neutral conditions. Neutral water splitting avoids corrosion problems and simplifies the system, posing an urgent need for more efficient catalysts. In Fig. 8, a comparison of the materials used in neutral pH with other catalysts under alkaline conditions (1 M KOH) is made. The average η_{10} for neutral conditions is 503 mV, which is the highest value compared with others. Lowering the pH to neutral or near-neutral causes a decrease in the hydroxide ion concentration; thereby, its activity also decreases. The best result was achieved with iridium doped Co–P ($\eta_{10} = 300$ mV, 1 M potassium borate (pH 9.2)). Usually, phosphides attained a value of overpotential below 503 mV. Density functional theory (DFT) calculations indicate that Co–P has much less free energy for conversion of MO to MOOH, which is the rate-determining step in the four elementary water oxidation reactions [206].

8. Summary

This review summarizes and highlights recent progress in the development of efficient and low-cost oxygen evolution electrocatalysts for electrolysis of water in an alkaline and a neutral environment. This field has been developing rapidly over the last 10 years, as there is an urgent need to replace the expensive and rare metals that currently represent the state-of-the-art in this field. The main problem is that the OER is a significant source of energy loss due to the sluggish kinetics as it is a complex 4-electron process. Therefore, it is still a challenge to design a suitable effective electrocatalyst. Ni, Co, Fe and their combinations are the most extensively studied transition metals in this respect. In agreement with the nature of the electrode reaction studied, the largest group of related studies is focused on the oxides of these metals. In recent years, there has been a growing interest in phosphides and selenides. As demonstrated in this paper, both phosphides and selenides can surpass the non-platinum oxides and, more importantly, even RuO_2. Moreover, the catalytic activity of all these materials can be further enhanced by the preparation of nano-sized structures. These structures have high specific surface areas, abundant active sites and can increase the charge transfer rate. It must be emphasized at this point that all aspects, like composition, material preparation/processing, and its morphology, are responsible for the resulting catalyst's electrochemical activity, selectivity, and stability. Thus, the development of advanced catalysts requires precise control of all these factors.

Declaration of competing interest

The authors declare that they have no known competing financial interests or personal relationships that could have appeared to influence the work reported in this paper.

Acknowledgement

This project has received funding from the European Union's Horizon 2020 research and innovation programme under grant agreement No 862509.

Appendix A. Supplementary data

Supplementary data to this article can be found online at https://doi.org/10.1016/j.jpowsour.2021.230072.

References

[1] S.P.S. Badwal, et al., Emerging electrochemical energy conversion and storage technologies, Front. Chem. 2 (79) (2014).
[2] P. Millet, 18 - membrane electrolysers for hydrogen (H2) production, in: A. Basile, S.P. Nunes (Eds.), Advanced Membrane Science and Technology for Sustainable Energy and Environmental Applications, Woodhead Publishing, 2011, pp. 568–609.
[3] P. Millet, S. Grigoriev, Chapter 2 - water electrolysis technologies, in: L. M. Gandía, G. Arzamendi, P.M. Diéguez (Eds.), Renewable Hydrogen Technologies, Elsevier, Amsterdam, 2013, pp. 19–41.
[4] L.M.d. Silva, M.H.P. Santana, J.F.C. Boodts, Electrochemistry and green chemical processes: electrochemical ozone production 26, Química Nova, 2003, pp. 880–888.
[5] M. Xiao, et al., Onsite deposition of self-repairing biomimetic nanostructured Ni catalysts with improved electrocatalysis toward glycerol oxidation for H2 production, Electrochim. Acta 178 (2015) 209–216.
[6] A. Iriondo, et al., Hydrogen production from glycerol over nickel catalysts supported on Al2O3 modified by Mg, Zr, Ce or La, Top. Catal. 49 (1) (2008) 46.
[7] P. Millet, 9 - hydrogen production by polymer electrolyte membrane water electrolysis, in: V. Subramani, A. Basile, T.N. Veziroğlu (Eds.), Compendium of Hydrogen Energy, Woodhead Publishing, Oxford, 2015, pp. 255–286.
[8] M. Ďurovič, J. Hnát, K. Bouzek, Electrocatalysts for the hydrogen evolution reaction in alkaline and neutral media. A comparative review, J. Power Sources 493 (2021) 229708.
[9] B. Hinnemann, et al., Biomimetic hydrogen Evolution: MoS2 nanoparticles as catalyst for hydrogen evolution, J. Am. Chem. Soc. 127 (15) (2005) 5308–5309.
[10] Z.W. Seh, et al., Two-dimensional molybdenum carbide (MXene) as an efficient electrocatalyst for hydrogen evolution, ACS Energy Letters 1 (3) (2016) 589–594.
[11] N.-T. Suen, et al., Electrocatalysis for the oxygen evolution reaction: recent development and future perspectives, Chem. Soc. Rev. 46 (2) (2017) 337–365.
[12] A.L. Strickler, D. Higgins, T.F. Jaramillo, Crystalline strontium iridate particle catalysts for enhanced oxygen evolution in acid, ACS Appl. Energy Mater. 2 (8) (2019) 5490–5498.
[13] J. Mohammed Ibrahim, X. Sun, Recent progress on earth abundant electrocatalysts for oxygen evolution reaction (OER) in alkaline medium to achieve efficient water splitting – a review, J. Power Sources 400 (2018) 31–68.
[14] Y. Yan, et al., A review on noble-metal-free bifunctional heterogeneous catalysts for overall electrochemical water splitting, J. Mater. Chem. 4 (45) (2016) 17587–17603.
[15] C. Hu, L. Zhang, J. Gong, Recent progress made in the mechanism comprehension and design of electrocatalysts for alkaline water splitting, Energy Environ. Sci. 12 (9) (2019) 2620–2645.
[16] X. Li, Z. Cheng, X. Wang, Understanding the Mechanism of Oxygen Evolution Reaction (OER) with the Consideration of Spin, 2020.
[17] G. Bronoel, J. Reby, Mechanism of oxygen evolution in basic medium at a nickel electrode, Electrochim. Acta 25 (7) (1980) 973–976.
[18] N. Yuan, et al., A review on non-noble metal based electrocatalysis for the oxygen evolution reaction, Arab. J. Chem. 13 (2) (2020) 4294–4309.
[19] H. Dau, et al., The mechanism of water oxidation: from electrolysis via, Homogeneous Biol. Catal. 2 (7) (2010) 724–761.
[20] L. Zhang, H. Zhao, D. Wilkinson, X. Sun, J. Zhang, Electrochemical Water Electrolysis, 2020 (Boca Raton).
[21] X. Huang, et al., An essential descriptor for the oxygen evolution reaction on reducible metal oxide surfaces, Chem. Sci. 10 (11) (2019) 3340–3345.
[22] K.S. Exner, Design criteria for oxygen evolution electrocatalysts from first principles: introduction of a unifying material-screening approach, ACS Appl. Energy Mater. 2 (11) (2019) 7991–8001.
[23] V. Viswanathan, H.A. Hansen, Unifying solution and surface electrochemistry: limitations and opportunities in surface electrocatalysis, Top. Catal. 57 (1) (2014) 215–221.
[24] J.K. Nørskov, et al., Origin of the overpotential for oxygen reduction at a fuel-cell cathode, J. Phys. Chem. B 108 (46) (2004) 17886–17892.
[25] P. Quaino, et al., Volcano plots in hydrogen electrocatalysis – uses and abuses, Beilstein J. Nanotechnol. 5 (2014) 846–854.
[26] A.R. Zeradjanin, et al., A critical review on hydrogen evolution electrocatalysis: Re-exploring the volcano-relationship 28 (10) (2016) 2256–2269.
[27] K.S. Exner, A universal descriptor for the screening of electrode materials for multiple-electron processes: beyond the thermodynamic overpotential, ACS Catal. 10 (21) (2020) 12607–12617.

[28] O. Piqué, F. Illas, F. Calle-Vallejo, Designing water splitting catalysts using rules of thumb: advantages, dangers and alternatives, Phys. Chem. Chem. Phys. 22 (13) (2020) 6797–6803.
[29] K.S. Exner, Recent progress in the development of screening methods to identify electrode materials for the oxygen evolution reaction 30 (42) (2020), 2005060.
[30] E. Fabbri, et al., Developments and perspectives of oxide-based catalysts for the oxygen evolution reaction, Catal. Sci. Technol. 4 (11) (2014) 3800–3821.
[31] J. Cruz, et al., Preparation and characterization of ruo(2) catalysts for oxygen evolution in a solid polymer electrolyte, Int. J. Electrochem. Sci. 7 (2011) 6607.
[32] K.A. Stoerzinger, et al., Orientation-dependent oxygen evolution activities of rutile IrO2 and RuO2, J. Phys. Chem. Lett. 5 (10) (2014) 1636–1641.
[33] Z. Ma, et al., Reaction mechanism for oxygen evolution on RuO2, IrO2, and RuO2@IrO2 core-shell nanocatalysts, J. Electroanal. Chem. 819 (2018) 296–305.
[34] K.S. Exner, Overpotential-dependent volcano plots to assess activity trends in the competing chlorine and oxygen evolution reactions 7 (6) (2020) 1448–1455.
[35] D. Krishnamurthy, V. Sumaria, V. Viswanathan, Maximal predictability approach for identifying the right descriptors for electrocatalytic reactions, J. Phys. Chem. Lett. 9 (3) (2018) 588–595.
[36] L.G.V. Briquet, et al., A new type of scaling relations to assess the accuracy of computational predictions of catalytic activities applied to the oxygen evolution reaction 9 (7) (2017) 1261–1268.
[37] Y. Lee, et al., Synthesis and activities of rutile IrO2 and RuO2 nanoparticles for oxygen evolution in acid and alkaline solutions, J. Phys. Chem. Lett. 3 (3) (2012) 399–404.
[38] H. Osgood, et al., Transition metal (Fe, Co, Ni, and Mn) oxides for oxygen reduction and evolution bifunctional catalysts in alkaline media, Nano Today 11 (5) (2016) 601–625.
[39] M. Tahir, et al., Electrocatalytic oxygen evolution reaction for energy conversion and storage: a comprehensive review, Nano Energy 37 (2017) 136–157.
[40] Y. Yang, et al., Efficient electrocatalytic oxygen evolution on amorphous nickel–cobalt binary oxide nanoporous layers, ACS Nano 8 (9) (2014) 9518–9523.
[41] Z. Qiu, et al., Direct observation of active catalyst surface phases and the effect of dynamic self-optimization in NiFe-layered double hydroxides for alkaline water splitting, Energy Environ. Sci. 12 (2) (2019) 572–581.
[42] S. Jin, Are metal chalcogenides, nitrides, and phosphides oxygen evolution catalysts or bifunctional catalysts? ACS Energy Letters 2 (8) (2017) 1937–1938.
[43] U. Müller, Inorganic Structural Chemistry, second ed., Wiley, Chichester, 2007.
[44] M.E.G. Lyons, M.P. Brandon, A comparative study of the oxygen evolution reaction on oxidised nickel, cobalt and iron electrodes in base, J. Electroanal. Chem. 641 (1) (2010) 119–130.
[45] S. Palmas, et al., Behavior of cobalt oxide electrodes during oxidative processes in alkaline medium, Electrochim. Acta 53 (2) (2007) 400–406.
[46] L. Trotochaud, et al., Solution-cast metal oxide thin film electrocatalysts for oxygen evolution, J. Am. Chem. Soc. 134 (41) (2012) 17253–17261.
[47] B.M. Hunter, J.R. Winkler, H.B. Gray, Iron is the active site in nickel/iron water oxidation electrocatalysts, Molecules 23 (4) (2018) 903.
[48] Y. Cheng, S.P. Jiang, Advances in electrocatalysts for oxygen evolution reaction of water electrolysis-from metal oxides to carbon nanotubes, Prog. Nat. Sci.: Mater. Int. 25 (6) (2015) 545–553.
[49] R. Subbaraman, et al., Trends in activity for the water electrolyser reactions on 3d M(Ni,Co,Fe,Mn) hydr(oxy)oxide catalysts, Nat. Mater. 11 (6) (2012) 550–557.
[50] X. Liu, et al., Rational composition and structural design of in situ grown nickel-based electrocatalysts for efficient water electrolysis, J. Mater. Chem. 4 (1) (2016) 167–172.
[51] L. Yu, et al., Hierarchical hollow nanoprisms based on ultrathin Ni-Fe layered double hydroxide nanosheets with enhanced electrocatalytic activity towards oxygen evolution 57 (1) (2018) 172–176.
[52] P.-c. Wang, et al., NiFe hydroxide supported on hierarchically porous nickel mesh as a high-performance bifunctional electrocatalyst for water splitting at large current density 12 (17) (2019) 4038–4045.
[53] M. Li, et al., Facile synthesis of electrospun MFe2O4 (M = Co, Ni, Cu, Mn) spinel nanofibers with excellent electrocatalytic properties for oxygen evolution and hydrogen peroxide reduction, Nanoscale 7 (19) (2015) 8920–8930.
[54] S. Diodati, et al., Green and low temperature synthesis of nanocrystalline transition metal ferrites by simple wet chemistry routes, Nano Research 7 (7) (2014) 1027–1042.
[55] T. Pandiarajan, S. Ravichandran, L.J. Berchmans, Enhancing the electro catalytic activity of manganese ferrite through cerium substitution for oxygen evolution in KOH solutions, RSC Adv. 4 (109) (2014) 64364–64370.
[56] D.H. Taffa, et al., Photoelectrochemical and theoretical investigations of spinel type ferrites (MxFe3-xO4) for water splitting: a mini-review, J. Photon. Energy 7 (1) (2017), 012009.
[57] J.P. Singh, N.K. Singh, R.N. Singh, Electrocatalytic activity of metal—substituted Fe3O4 obtained at low temperature for O2 evolution, Int. J. Hydrogen Energy 24 (5) (1999) 433–439.
[58] N.K. Singh, et al., Electrocatalytic properties of spinel-type MnFe3 – O4synthesized below 100 °C for oxygen evolution in KOH solutions, J. Chem. Soc., Faraday Trans. 92 (13) (1996) 2397–2400.
[59] G.-C. Chen, et al., Microwave-assisted facile synthesis of cobaltiron oxide nanocomposites for oxygen production using alkaline anion exchange membrane water electrolysis, Int. J. Hydrogen Energy 44 (21) (2019) 10174–10181.
[60] R. Yadav, N.K. Singh, Electrocatalytic activity of NixFe3-xO4 ($0 \leq x \leq 1.5$) film electrode for oxygen evolution in KOH solutions, Indian J. Chem. Technol. 25 (2) (2018) 189–195.
[61] J. Zhao, et al., Highly-active oxygen evolution electrocatalyzed by an Fe-doped NiCr2O4 nanoparticle film, Chem. Commun. 54 (43) (2018) 5462–5465.
[62] A. Singh Anindita, R.N. Singh, Effect of V substitution at B-site on the physicochemical and electrocatalytic properties of spinel-type NiFe2O4 towards O2 evolution in alkaline solutions, Int. J. Hydrogen Energy 35 (8) (2010) 3243–3248.
[63] R.N. Singh, et al., New NiFe2−xCrxO4 spinel films for O2 evolution in alkaline solutions, Electrochim. Acta 51 (25) (2006) 5515–5523.
[64] R.N. Singh, et al., Preparation and characterization of CuFe2 - x Crx O4 ($0 \leq x \leq 1.0$) nano spinels for electrocatalysis of oxygen evolution in alkaline solutions, Int. J. Hydrogen Energy 32 (1) (2007) 11–16.
[65] R.N. Singh, et al., Effect of partial substitution of Cr on electrocatalytic properties of CoFe2O4 towards O2-evolution in alkaline medium, Int. J. Hydrogen Energy 31 (6) (2006) 701–707.
[66] R.N. Singh, et al., Effect of partial substitution of Cr on electrocatalytic properties of MnFe2O4 towards O2-evolution in alkaline medium, Int. J. Hydrogen Energy 31 (10) (2006) 1372–1378.
[67] J.Y.C. Chen, et al., Inverse spinel NiFeAlO4 as a highly active oxygen evolution electrocatalyst: promotion of activity by a redox-inert metal ion, Energy Environ. Sci. 7 (4) (2014) 1382–1386.
[68] M. Gong, H. Dai, A mini review of NiFe-based materials as highly active oxygen evolution reaction electrocatalysts, Nano Research 8 (1) (2015) 23–39.
[69] W. Ma, et al., A superlattice of alternately stacked Ni–Fe hydroxide nanosheets and graphene for efficient splitting of water, ACS Nano 9 (2) (2015) 1977–1984.
[70] F. Dionigi, et al., In-situ structure and catalytic mechanism of NiFe and CoFe layered double hydroxides during oxygen evolution, Nat. Commun. 11 (1) (2020) 2522.
[71] B.M. Hunter, et al., Effect of interlayer anions on [NiFe]-LDH nanosheet water oxidation activity, Energy Environ. Sci. 9 (5) (2016) 1734–1743.
[72] J. Yu, et al., Preparation of two dimensional layered double hydroxide nanosheets and their applications, Chem. Soc. Rev. 46 (19) (2017) 5950–5974.
[73] S.I. Córdoba, et al., The effect of iron hydroxide on nickelous hydroxide electrodes with emphasis on the oxygen evolution reaction, Electrochim. Acta 32 (5) (1987) 749–755.
[74] J. Guo, et al., Electrodepositing Pd on NiFe layered double hydroxide for improved water electrolysis, Mater. Chem. Front. 3 (5) (2019) 842–850.
[75] K. Nejati, et al., A highly active oxygen evolution electrocatalyst: Ni-Fe-layered double hydroxide intercalated with the Molybdate and Vanadate anions, Int. J. Hydrogen Energy 44 (29) (2019) 14842–14852.
[76] G.-J. Hwang, B.-M. Gil, C.-H. Ryu, Preparation of the electrode using NiFe2O4 powder for the alkaline water electrolysis, J. Ind. Eng. Chem. 48 (2017) 242–248.
[77] M. Orlandi, et al., Pulsed-laser deposition of nanostructured iron oxide catalysts for efficient water oxidation, ACS Appl. Mater. Interfaces 6 (9) (2014) 6186–6190.
[78] M.D. Merrill, R.C. Dougherty, Metal oxide catalysts for the evolution of O2 from H2O, J. Phys. Chem. C 112 (10) (2008) 3655–3666.
[79] L. Kuai, et al., A reliable aerosol-spray-assisted approach to produce and optimize amorphous metal oxide catalysts for electrochemical water splitting 53 (29) (2014) 7547–7551.
[80] Y. Qiu, L. Xin, W. Li, Electrocatalytic oxygen evolution over supported small amorphous Ni–Fe nanoparticles in alkaline electrolyte, Langmuir 30 (26) (2014) 7893–7901.
[81] R. Pittkowski, P. Krtil, J. Rossmeisl, Rationality in the new oxygen evolution catalyst development, Curr. Opin. Electrochem. 12 (2018) 218–224.
[82] X. Lu, C. Zhao, Electrodeposition of hierarchically structured three-dimensional nickel–iron electrodes for efficient oxygen evolution at high current densities, Nat. Commun. 6 (1) (2015) 6616.
[83] R.M. Ramsundar, et al., Co3O4 nanorods—efficient non-noble metal electrocatalyst for oxygen evolution at neutral pH, Electrocatalysis 6 (4) (2015) 331–340.
[84] T. Shinagawa, M.T.-K. Ng, K. Takanabe, Electrolyte engineering towards efficient water splitting at mild pH 10 (21) (2017) 4155–4162.
[85] M. Chen, et al., An iron-based film for highly efficient electrocatalytic oxygen evolution from neutral aqueous solution, ACS Appl. Mater. Interfaces 7 (39) (2015) 21852–21859.
[86] D.A. Islam, et al., Ag-Nanoparticle-Anchored rGO-coated MIL-88B(Fe) hybrids as robust electrocatalysts for the highly efficient oxygen evolution reaction at neutral pH 4 (12) (2017) 3110–3118.
[87] J. Masud, et al., Copper selenides as high-efficiency electrocatalysts for oxygen evolution reaction, ACS Appl. Energy Mater. 1 (8) (2018) 4075–4083.
[88] Y. Wang, et al., Electrocatalysis: reduced mesoporous Co3O4 nanowires as efficient water oxidation electrocatalysts and supercapacitor electrodes, Adv. Energy Mater. 4 (16) (2014) 1400696.
[89] N. Dahal, I.A. Ibarra, S.M. Humphrey, High surface area mesoporous Co3O4 from a direct soft template route, J. Mater. Chem. 22 (25) (2012) 12675–12681.
[90] A.J. Esswein, et al., Size-dependent activity of Co3O4 nanoparticle anodes for alkaline water electrolysis, J. Phys. Chem. C 113 (33) (2009) 15068–15072.
[91] X. Deng, H. Tüysüz, Cobalt-oxide-based materials as water oxidation catalyst: recent progress and challenges, ACS Catal. 4 (10) (2014) 3701–3714.
[92] J.B. Gerken, et al., Electrochemical water oxidation with cobalt-based electrocatalysts from pH 0–14: the thermodynamic basis for catalyst structure, stability, and activity, J. Am. Chem. Soc. 133 (36) (2011) 14431–14442.
[93] H.H. Pham, et al., Surface proton hopping and fast-kinetics pathway of water oxidation on Co3O4 (001) surface, ACS Catal. 6 (8) (2016) 5610–5617.
[94] J. Wu, et al., Co3O4 nanocrystals on single-walled carbon nanotubes as a highly efficient oxygen-evolving catalyst, Nano Research 5 (8) (2012) 521–530.

[95] L. Wu, et al., Stable cobalt nanoparticles and their monolayer array as an efficient electrocatalyst for oxygen evolution reaction, J. Am. Chem. Soc. 137 (22) (2015) 7071–7074.

[96] L. Li, et al., Hierarchically porous Co3O4 architectures with honeycomb-like structures for efficient oxygen generation from electrochemical water splitting, J. Power Sources 294 (2015) 103–111.

[97] C. Bocca, et al., Oxygen evolution on Co3O4 and Li-doped Co3O4 coated electrodes in an alkaline solution, Int. J. Hydrogen Energy 24 (8) (1999) 699–707.

[98] J.A. Koza, et al., Electrodeposition of crystalline Co3O4—a catalyst for the oxygen evolution reaction, Chem. Mater. 24 (18) (2012) 3567–3573.

[99] D. Yan, et al., Engineering the electronic structure of Co3O4 by carbon-doping for efficient overall water splitting, Electrochim. Acta 303 (2019) 316–322.

[100] E. Antolini, E. Zhecheva, Lithiation of spinel cobalt oxide by solid state reaction of Li2CO3 and Co3O4: an EPR study, Mater. Lett. 35 (5) (1998) 380–382.

[101] H. Jin, et al., Synthesis of Li-doped Co3O4 truncated octahedra with improved performances in CO oxidation and lithium ion batteries, Sci. China Technol. Sci. 56 (1) (2013) 8–12.

[102] I. Nikolov, et al., Electrocatalytic activity of spinel related cobalties MxCo3−xO4 (M = Li, Ni, Cu) in the oxygen evolution reaction, J. Electroanal. Chem. 429 (1) (1997) 157–168.

[103] F. Švegl, et al., Characterization of spinel Co3O4 and Li-doped Co3O4 thin film electrocatalysts prepared by the sol–gel route, Electrochim. Acta 45 (25) (2000) 4359–4371.

[104] P. Rasiyah, A.C.C. Tseung, A mechanistic study of oxygen evolution on Li-doped Co3O4, J. Electrochem. Soc. 130 (2) (1983) 365–368.

[105] M. Hamdani, et al., Physicochemical and electrocatalytic properties of Li-Co3O4 anodes prepared by chemical spray pyrolysis for application in alkaline water electrolysis, Electrochim. Acta 49 (9) (2004) 1555–1563.

[106] X. Wu, K. Scott, A Li-doped Co3O4 oxygen evolution catalyst for non-precious metal alkaline anion exchange membrane water electrolysers, Int. J. Hydrogen Energy 38 (8) (2013) 3123–3129.

[107] R.N. Singh, et al., Sol-gel derived spinel MxCo3−xO4 (M=Ni, Cu; 0≤x≤1) films and oxygen evolution, Electrochim. Acta 45 (12) (2000) 1911–1919.

[108] P. Rasiyah, A.C.C. Tseung, D.B. Hibbert, A mechanistic study of oxygen evolution on NiCo2O4: I. Formation of higher oxides, J. Electrochem. Soc. 129 (8) (1982) 1724–1727.

[109] X. Wu, K. Scott, CuxCo3−xO4 ($0 \leq x < 1$) nanoparticles for oxygen evolution in high performance alkaline exchange membrane water electrolysers, J. Mater. Chem. 21 (33) (2011) 12344–12351.

[110] X. Wu, K. Scott, A non-precious metal bifunctional oxygen electrode for alkaline anion exchange membrane cells, J. Power Sources 206 (2012) 14–19.

[111] R.N. Singh, et al., Novel electrocatalysts for generating oxygen from alkaline water electrolysis, Electrochem. Commun. 9 (6) (2007) 1369–1373.

[112] A. QayoomMugheri, et al., Co3O4/NiO bifunctional electrocatalyst for water splitting, Electrochim. Acta 306 (2019) 9–17.

[113] X. Liu, et al., Au/NiCo2O4 arrays with high activity for water oxidation, ChemCatChem 6 (9) (2014) 2501–2506.

[114] Y. Zhang, et al., Rock salt type NiCo2O3 supported on ordered mesoporous carbon as a highly efficient electrocatalyst for oxygen evolution reaction, Appl. Catal. B Environ. 256 (2019) 117852.

[115] Y. Yang, et al., Hierarchical nanoassembly of MoS2/Co9S8/Ni3S2/Ni as a highly efficient electrocatalyst for overall water splitting in a wide pH range, J. Am. Chem. Soc. 141 (26) (2019) 10417–10430.

[116] J. Li, et al., Co9S8–Ni3S2 heterointerfaced nanotubes on Ni foam as highly efficient and flexible bifunctional electrodes for water splitting, Electrochim. Acta 299 (2019) 152–162.

[117] F.M. Sapountzi, et al., Electrocatalysts for the generation of hydrogen, oxygen and synthesis gas, Prog. Energy Combust. Sci. 58 (2017) 1–35.

[118] Y. Zhu, et al., Spinel NiCo2O4 for use as a high-performance supercapacitor electrode material: understanding of its electrochemical properties, J. Power Sources 267 (2014) 888–900.

[119] C. Jin, et al., Facile synthesis and excellent electrochemical properties of NiCo2O4 spinel nanowire arrays as a bifunctional catalyst for the oxygen reduction and evolution reaction, J. Mater. Chem. 1 (39) (2013) 12170–12177.

[120] Z. Zheng, et al., Efficient and stable NiCo2O4/VN nanoparticle catalyst for electrochemical water oxidation, ACS Sustain. Chem. Eng. 6 (9) (2018) 11473–11479.

[121] J. Lin, et al., Rich P vacancies modulate Ni2P/Cu3P interfaced nanosheets for electrocatalytic alkaline water splitting, J. Colloid Interface Sci. 564 (2020) 37–42.

[122] S.V. Devaguptapu, et al., Morphology control of carbon-free spinel NiCo2O4 catalysts for enhanced bifunctional oxygen reduction and evolution in alkaline media, ACS Appl. Mater. Interfaces 9 (51) (2017) 44567–44578.

[123] L. Yang, et al., A comparative study of NiCo2O4 catalyst supported on Ni foam and from solution residuals fabricated by a hydrothermal approach for electrochemical oxygen evolution reaction, Chem. Commun. 54 (93) (2018) 13151–13154.

[124] C. Bocca, et al., NICKEL–COBALT oxide-coated electrodes: influence of the preparation technique on oxygen evolution reaction (OER) in an alkaline solution, Int. J. Hydrogen Energy 24 (1) (1999) 21–26.

[125] S.K. Tiwari, et al., Active thin NiCo2O4 film prepared on nickel by spray pyrolysis for oxygen evolution, Int. J. Hydrogen Energy 20 (1) (1995) 9–15.

[126] M. El Baydi, et al., High specific surface area nickel mixed oxide powders LaNiO3 (perovskite) and NiCo2O4 (spinel) via sol-gel type routes for oxygen electrocatalysis in alkaline media, J. Solid State Chem. 116 (1) (1995) 157–169.

[127] D. Chanda, et al., Optimization of synthesis of the nickel-cobalt oxide based anode electrocatalyst and of the related membrane-electrode assembly for alkaline water electrolysis, J. Power Sources 347 (2017) 247–258.

[128] H. Lin, et al., Cobalt-based layered double hydroxides as oxygen evolving electrocatalysts in neutral electrolyte, Front. Mater. Sci. 6 (2) (2012) 142–148.

[129] Y. Zhang, et al., Co–Ni layered double hydroxides for water oxidation in neutral electrolyte, Phys. Chem. Chem. Phys. 15 (19) (2013) 7363–7369.

[130] H. Fang, et al., Prussian blue analog-derived 2D ultrathin CoFe2O4 nanosheets as high-activity electrocatalysts for the oxygen evolution reaction in alkaline and neutral media, J. Mater. Chem. 7 (13) (2019) 7328–7332.

[131] Y. Zhang, et al., Atomic iridium incorporated in cobalt hydroxide for efficient oxygen evolution catalysis in neutral electrolyte, Adv. Energy Mater. 30 (18) (2018) 1707522.

[132] P. Cai, et al., Oxygen-containing amorphous cobalt sulfide porous nanocubes as high-activity electrocatalysts for the oxygen evolution reaction in an alkaline/neutral medium, Angew. Chem. 56 (17) (2017) 4858–4861.

[133] M.A. Kirsanova, et al., Bifunctional OER/ORR catalytic activity in the tetrahedral YBaCo4O7.3 oxide, J. Mater. Chem. 7 (1) (2019) 330–341.

[134] S. Gupta, et al., Bifunctional perovskite oxide catalysts for oxygen reduction and evolution in alkaline media, Chem. Asian J. 11 (1) (2016) 10–21.

[135] X. Cheng, et al., Oxygen evolution reaction on La1–xSrxCoO3 perovskites: a combined experimental and theoretical study of their structural, electronic, and electrochemical properties, Chem. Mater. 27 (22) (2015) 7662–7672.

[136] X. Wang, et al., Eg occupancy as an effective descriptor for the catalytic activity of perovskite oxide-based peroxidase mimics, Nat. Commun. 10 (1) (2019) 704.

[137] H.S. Kushwaha, et al., CaCu3Ti4O12: a bifunctional perovskite electrocatalyst for oxygen evolution and reduction reaction in alkaline medium, Electrochim. Acta 252 (2017) 532–540.

[138] Y. Matsumoto, Oxygen evolution on La1−xSrxFe1−yCoyO3 series oxides, J. Electrochem. Soc. 127 (11) (1980) 2360.

[139] K.S. Exner, H. Over, Beyond the rate-determining step in the oxygen evolution reaction over a single-crystalline IrO2(110) model electrode: kinetic scaling relations, ACS Catal. 9 (8) (2019) 6755–6765.

[140] J.O.M. Bockris, T. Otagawa, Mechanism of oxygen evolution on perovskites, J. Phys. Chem. 87 (15) (1983) 2960–2971.

[141] I.C. Man, et al., Universality in oxygen evolution electrocatalysis on oxide surfaces 3 (7) (2011) 1159–1165.

[142] B. Han, et al., Iron-based perovskites for catalyzing oxygen evolution reaction, J. Phys. Chem. C 122 (15) (2018) 8445–8454.

[143] F. Cordero, F. Craciun, F. Trequattrini, Ionic mobility and phase transitions in perovskite oxides for energy application, Challenges 8 (2017) 5.

[144] W.T. Hong, et al., Toward the rational design of non-precious transition metal oxides for oxygen electrocatalysis, Energy Environ. Sci. 8 (5) (2015) 1404–1427.

[145] S. Yagi, et al., Covalency-reinforced oxygen evolution reaction catalyst, Nat. Commun. 6 (1) (2015) 8249.

[146] X.-Z. Fu, et al., Nickel oxyhydroxides with various oxidation states prepared by chemical oxidation of spherical β-Ni(OH)2, Solid State Ionics 178 (13) (2007) 987–993.

[147] H. Sun, et al., Smart control of composition for double perovskite electrocatalysts toward enhanced oxygen evolution reaction 12 (23) (2019) 5111–5116.

[148] B. Han, et al., Activity and stability trends of perovskite oxides for oxygen evolution catalysis at neutral pH, Phys. Chem. Chem. Phys. 17 (35) (2015) 22576–22580.

[149] H. Taguchi, M. Shimada, M. Koizumi, The effect of oxygen vacancy on the magnetic properties in the system SrCoO3−δ ($0 < \delta < 0.5$), J. Solid State Chem. 29 (2) (1979) 221–225.

[150] K.J. May, et al., Influence of oxygen evolution during water oxidation on the surface of perovskite oxide catalysts, J. Phys. Chem. Lett. 3 (22) (2012) 3264–3270.

[151] S.K. Tiwari, P. Chartier, R.N. Singh, Preparation of perovskite-type oxides of cobalt by the malic acid aided process and their electrocatalytic surface properties in relation to oxygen evolution, J. Electrochem. Soc. 142 (1) (1995) 148–153.

[152] R.N. Singh, B. Lal, High surface area lanthanum cobaltate and its A and B sites substituted derivatives for electrocatalysis of O2 evolution in alkaline solution, Int. J. Hydrogen Energy 27 (1) (2002) 45–55.

[153] A.N. Jain, et al., Low-temperature synthesis of perovskite-type oxides of lanthanum and cobalt and their electrocatalytic properties for oxygen evolution in alkaline solutions, J. Chem. Soc., Faraday Trans. 91 (12) (1995) 1871–1875.

[154] A. Grimaud, et al., Double perovskites as a family of highly active catalysts for oxygen evolution in alkaline solution, Nat. Commun. 4 (1) (2013) 2439.

[155] A. Grimaud, et al., Oxygen evolution activity and stability of Ba6Mn5O16, Sr4Mn2CoO9, and Sr6Co5O15: the influence of transition metal coordination, J. Phys. Chem. C 117 (49) (2013) 25926–25932.

[156] A. Ashok, et al., Combustion synthesis of bifunctional LaMO3 (M=Cr, Mn, Fe, Co, Ni) perovskites for oxygen reduction and oxygen evolution reaction in alkaline media, J. Electroanal. Chem. 809 (2018) 22–30.

[157] Z. Wu, et al., Effect of Sr doping on the electrochemical properties of bi-functional oxygen electrode PrBa1−xSrxCo2O5+δ, J. Power Sources 334 (2016) 86–93.

[158] C. Su, et al., SrCo0.9Ti0.1O3−δ as a new electrocatalyst for the oxygen evolution reaction in alkaline electrolyte with stable performance, ACS Appl. Mater. Interfaces 7 (32) (2015) 17663–17670.

[159] X. Xu, et al., Toward enhanced oxygen evolution on perovskite oxides synthesized from different approaches: a case study of Ba0.5Sr0.5Co0.8Fe0.2O3−δ, Electrochim. Acta 219 (2016) 553–559.

[160] B.R. Wygant, et al., Structural and catalytic effects of iron- and scandium-doping on a strontium cobalt oxide electrocatalyst for water oxidation, ACS Catal. 6 (2) (2016) 1122–1133.

[161] Z. Zhang, et al., Boosting overall water splitting via FeOOH nanoflake-decorated PrBa0.5Sr0.5Co2O5+δ nanorods, ACS Appl. Mater. Interfaces 10 (44) (2018) 38032–38041.

[162] C.B. Njoku, R.J. Kriek, Application of Sm0.8Sr0.2Fe1-xCoxO3-δ (x = 0.2, 0.5, 0.8) perovskite for the oxygen evolution reaction in alkaline media, Electrocatalysis 10 (4) (2019) 305–313.

[163] Y. Zhu, et al., SrNb0.1Co0.7Fe0.2O3−δ perovskite as a next-generation electrocatalyst for oxygen evolution in alkaline solution 54 (13) (2015) 3897–3901.

[164] W. Zhou, et al., High activity and durability of novel perovskite electrocatalysts for water oxidation, Mater. Horiz. 2 (5) (2015) 495–501.

[165] K. Zhu, et al., Perovskites decorated with oxygen vacancies and Fe–Ni alloy nanoparticles as high-efficiency electrocatalysts for the oxygen evolution reaction, J. Mater. Chem. 5 (37) (2017) 19836–19845.

[166] E. Omari, M. Omari, Cu-doped GdFeO3 perovskites as electrocatalysts for the oxygen evolution reaction in alkaline media, Int. J. Hydrogen Energy 44 (54) (2019) 28769–28779.

[167] W. Wang, et al., An excellent OER electrocatalyst of cubic SrCoO3−δ prepared by a simple F-doping strategy, J. Mater. Chem. 7 (20) (2019) 12538–12546.

[168] C.C. Wang, et al., A highly active and stable La0.5Sr0.5Ni0.4Fe0.6O3-δ perovskite electrocatalyst for oxygen evolution reaction in alkaline media, Electrochim. Acta 246 (2017) 997–1003.

[169] J. Balej, Electrocatalysts for oxygen evolution in advanced water electrolysis, Int. J. Hydrogen Energy 10 (2) (1985) 89–99.

[170] W. Zhou, J. Sunarso, Enhancing Bi-functional electrocatalytic activity of perovskite by temperature shock: a case study of LaNiO3−δ, J. Phys. Chem. Lett. 4 (17) (2013) 2982–2988.

[171] X. Wu, et al., Perovskite oxide/carbon nanotube hybrid bifunctional electrocatalysts for overall water splitting, Electrochim. Acta 286 (2018) 47–54.

[172] R.N. Singh, et al., Physicochemical and electrocatalytic properties of LaNiO3 prepared by a low-temperature route for anode application in alkaline water electrolysis, J. Appl. Electrochem. 25 (12) (1995) 1133–1138.

[173] A. Nemudry, P. Rudolf, R. Schöllhorn, Topotactic electrochemical redox reactions of the defect perovskite SrCoO2.5+x, Chem. Mater. 8 (9) (1996) 2232–2238.

[174] L.Q. Zhou, et al., A high-performance oxygen evolution catalyst in neutral-pH for sunlight-driven CO2 reduction, Nat. Commun. 10 (1) (2019) 4081.

[175] X. Cao, E. Johnson, M. Nath, Identifying high-efficiency oxygen evolution electrocatalysts from Co–Ni–Cu based selenides through combinatorial electrodeposition, J. Mater. Chem. 7 (16) (2019) 9877–9889.

[176] F. Gillot, L. Monconduit, M.L. Doublet, Electrochemical behaviors of binary and ternary manganese phosphides, Chem. Mater. 17 (23) (2005) 5817–5823.

[177] Y.-M. Hu, et al., One-pot hydrothermal synthesis of porous nickel cobalt phosphides with high conductivity for advanced energy conversion and storage, Electrochim. Acta 215 (2016) 114–125.

[178] Y. Feng, X.-Y. Yu, U. Paik, Nickel cobalt phosphides quasi-hollow nanocubes as an efficient electrocatalyst for hydrogen evolution in alkaline solution, Chem. Commun. 52 (8) (2016) 1633–1636.

[179] A. Dutta, N. Pradhan, Developments of metal phosphides as efficient OER precatalysts, J. Phys. Chem. Lett. 8 (1) (2017) 144–152.

[180] Y. Shao, X. Shi, H. Pan, Electronic, magnetic, and catalytic properties of thermodynamically stable two-dimensional transition-metal phosphides, Chem. Mater. 29 (20) (2017) 8892–8900.

[181] Y. Pei, et al., Recent developments of transition metal phosphides as catalysts in the energy conversion field, J. Mater. Chem. 6 (46) (2018) 23220–23243.

[182] Y. Yang, et al., Porous cobalt-based thin film as a bifunctional catalyst for hydrogen generation and oxygen generation, Adv. Mater. 27 (20) (2015) 3175–3180.

[183] N. Jiang, et al., Electrodeposited cobalt-phosphorous-derived films as competent bifunctional catalysts for overall water splitting, Angew. Chem. 54 (21) (2015) 6251–6254.

[184] M. Ledendecker, et al., The synthesis of nanostructured Ni5P4 films and their use as a non-noble bifunctional electrocatalyst for full water splitting, Angew. Chem. Int. Ed. 54 (42) (2015) 12361–12365.

[185] L.A. Stern, et al., Ni2P as a Janus catalyst for water splitting: the oxygen evolution activity of Ni2P nanoparticles, Energy Environ. Sci. 8 (8) (2015) 2347–2351.

[186] S. Yue, et al., Preparation of yolk–shell-structured CoxFe1−xP with enhanced OER performance, ChemSusChem 12 (19) (2019) 4461–4470.

[187] Y. Du, et al., Bimetallic CoFeP hollow microspheres as highly efficient bifunctional electrocatalysts for overall water splitting in alkaline media, Appl. Surf. Sci. 465 (2019) 816–823.

[188] H. Feng, et al., Electron density modulation of Fe1-xCoxP nanosheet arrays by iron incorporation for highly efficient water splitting, Nano Energy 67 (2020).

[189] L. Li, et al., Holey nanospheres of amorphous bimetallic phosphide electrodeposited on 3D porous Ni foam for efficient oxygen evolution, Appl. Surf. Sci. 479 (2019) 540–547.

[190] H. Sun, et al., Morphological and electronic tuning of Ni2P through iron doping toward highly efficient water splitting, ACS Catal. 9 (10) (2019) 8882–8892.

[191] W. Tang, et al., Boosting electrocatalytic water splitting via metal-metalloid combined modulation in quaternary Ni-Fe-P-B amorphous compound, Nano Research 13 (2) (2020) 447–454.

[192] B. Xu, et al., Anion-cation dual doping: an effective electronic modulation strategy of Ni2P for high-performance oxygen evolution, J. Energy Chem. 48 (2020) 116–121.

[193] Q. Xu, et al., Electrodeposition of NiS/Ni2P nanoparticles embedded in amorphous Ni(OH)2 nanosheets as an efficient and durable dual-functional electrocatalyst for overall water splitting, Int. J. Hydrogen Energy 45 (4) (2020) 2546–2556.

[194] H. Wang, et al., Self-assembled Ni2P/FeP heterostructural nanoparticles embedded in N-doped graphene nanosheets as highly efficient and stable multifunctional electrocatalyst for water splitting, Electrochim. Acta 318 (2019) 449–459.

[195] W. Xu, et al., A nanoporous metal phosphide catalyst for bifunctional water splitting, J. Mater. Chem. 6 (14) (2018) 5574–5579.

[196] E. Loni, M.H. Siadati, A. Shokuhfar, Mesoporous cobalt–cobalt phosphide electrocatalyst for water splitting, Mater. Today Energy 16 (2020).

[197] J. Masa, et al., Low overpotential water splitting using cobalt–cobalt phosphide nanoparticles supported on nickel foam, ACS Energy Letters 1 (6) (2016) 1192–1198.

[198] R.N. Wasalathanthri, et al., Electrodeposited copper–cobalt–phosphide: a stable bifunctional catalyst for both hydrogen and oxygen evolution reactions, ACS Sustain. Chem. Eng. 7 (3) (2019) 3092–3100.

[199] P. Karthika, et al., Synthesis of mesoporous Pt–Ru alloy particles with uniform sizes by sophisticated hard-templating method, Chem. Asian J. 8 (5) (2013) 902–907.

[200] A. Chunduri, et al., A unique amorphous cobalt-phosphide-boride bifunctional electrocatalyst for enhanced alkaline water-splitting, Appl. Catal. B Environ. 259 (2019) 118051.

[201] Z. Wu, et al., Element-specific restructuring of anion- and cation-substituted cobalt phosphide nanoparticles under electrochemical water-splitting conditions, ACS Catal. 9 (4) (2019) 2956–2961.

[202] F. Yu, et al., High-performance bifunctional porous non-noble metal phosphide catalyst for overall water splitting, Nat. Commun. 9 (1) (2018) 2551.

[203] Z. Chen, et al., Room-temperature preparation of cobalt-based electrocatalysts through simple solution treatment for selectively high-efficiency hydrogen evolution reaction in alkaline or acidic medium, J. Nanomater. (2018) 8124920.

[204] M.W. Kanan, D.G. Nocera, In situ formation of an oxygen-evolving catalyst in neutral water containing phosphate and Co2+, Science 321 (5892) (2008) 1072–1075.

[205] L. Xie, et al., High-performance electrolytic oxygen evolution in neutral media catalyzed by a cobalt phosphate nanoarray, Angew. Chem. 56 (4) (2017) 1064–1068.

[206] L. Zhang, et al., Co-based nanowire films as complementary hydrogen- and oxygen-evolving electrocatalysts in neutral electrolyte, Catal. Sci. Technol. 7 (13) (2017) 2689–2694.

[207] Y. Surendranath, M.W. Kanan, D.G. Nocera, Mechanistic studies of the oxygen evolution reaction by a cobalt-phosphate catalyst at neutral pH, J. Am. Chem. Soc. 132 (46) (2010) 16501–16509.

[208] H.S. Ahn, T.D. Tilley, Electrocatalytic water oxidation at neutral pH by a nanostructured Co(PO3)2 anode, Adv. Funct. Mater. 23 (2) (2013) 227–233.

[209] L. Cui, et al., In situ electrochemical surface derivation of cobalt phosphate from a Co(CO3)0.5(OH)·0.11H2O nanoarray for efficient water oxidation in neutral aqueous solution, Nanoscale 9 (11) (2017) 3752–3756.

[210] T. Liu, et al., Self-standing CoP nanosheets array: a three-dimensional bifunctional catalyst electrode for overall water splitting in both neutral and alkaline media 4 (8) (2017) 1840–1845.

[211] Z. Wang, Z. Lin, P. Diao, Hybrids of iridium–cobalt phosphates as a highly efficient electrocatalyst for the oxygen evolution reaction in neutral solution, Chem. Commun. 55 (20) (2019) 3000–3003.

[212] B. Zhang, et al., Bimetallic (FexNi1−x)2P nanoarrays as exceptionally efficient electrocatalysts for oxygen evolution in alkaline and neutral media, Nano Energy 38 (2017) 553–560.

[213] B. Zhang, et al., An alkaline electro-activated Fe–Ni phosphide nanoparticle-stack array for high-performance oxygen evolution under alkaline and neutral conditions, J. Mater. Chem. 5 (26) (2017) 13329–13335.

[214] A.T. Swesi, J. Masud, M. Nath, Nickel selenide as a high-efficiency catalyst for oxygen evolution reaction, Energy Environ. Sci. 9 (5) (2016) 1771–1782.

[215] K. Xu, et al., Understanding structure-dependent catalytic performance of nickel selenides for electrochemical water oxidation, ACS Catal. 7 (1) (2017) 310–315.

[216] X. Cao, J.E. Medvedeva, M. Nath, Copper cobalt selenide as a high-efficiency bifunctional electrocatalyst for overall water splitting: combined experimental and theoretical study, ACS Appl. Energy Mater. 3 (3) (2020) 3092–3103.

[217] J. Ding, et al., Mesoporous nickel selenide N-doped carbon as a robust electrocatalyst for overall water splitting, Electrochim. Acta 300 (2019) 93–101.

[218] S. Esmailzadeh, et al., Pulse electrodeposition of nickel selenide nanostructure as a binder-free and high-efficient catalyst for both electrocatalytic hydrogen and oxygen evolution reactions in alkaline solution, Electrochim. Acta 334 (2020) 135549.

[219] H. Kang, et al., Anion doped bimetallic selenide as efficient electrocatalysts for oxygen evolution reaction, Ceram. Int. 46 (3) (2020) 2792–2797.

[220] T. Liu, et al., An amorphous CoSe film behaves as an active and stable full water-splitting electrocatalyst under strongly alkaline conditions, Chem. Commun. 51 (93) (2015) 16683–16686.

[221] J. Zhang, et al., Self-supported porous NiSe2 nanowrinkles as efficient bifunctional electrocatalysts for overall water splitting, ACS Sustain. Chem. Eng. 6 (2) (2018) 2231–2239.

[222] P.F. Liu, et al., Surface engineering of nickel selenide for an enhanced intrinsic overall water splitting ability, Mater. Chem. Front. 2 (9) (2018) 1725–1731.

[223] L. Gui, et al., Integrated ultrafine Co0.85Se in carbon nanofibers: an efficient and robust bifunctional catalyst for oxygen electrocatalysis, Chem. European J. 26 (18) (2020) 4063–4069.
[224] Y. Zhong, et al., Regulating phase conversion from Ni3Se2 into NiSe in a bifunctional electrocatalyst for overall water-splitting enhancement, Chem. European J. 12 (9) (2019) 2008–2014.
[225] R. Bose, et al., A highly effective, stable oxygen evolution catalyst derived from transition metal selenides and phosphides, Particle & Particle Szst. Charact. 35 (8) (2018) 1800135.
[226] X. Cao, et al., Phase exploration and identification of multinary transition-metal selenides as high-efficiency oxygen evolution electrocatalysts through combinatorial electrodeposition, ACS Catal. 8 (9) (2018) 8273–8289.
[227] X. Cao, E. Johnson, M. Nath, Expanding multinary selenide based high-efficiency oxygen evolution electrocatalysts through combinatorial electrodeposition: case study with Fe–Cu–Co selenides, ACS Sustain. Chem. Eng. 7 (10) (2019) 9588–9600.
[228] C. Jiao, X. Bo, M. Zhou, Electrocatalytic water splitting at nitrogen-doped carbon layers-encapsulated nickel cobalt selenide, J. Energy Chem. 34 (2019) 161–170.
[229] I.H. Kwak, et al., CoSe2 and NiSe2 nanocrystals as superior bifunctional catalysts for electrochemical and photoelectrochemical water splitting, ACS Appl. Mater. Interfaces 8 (8) (2016) 5327–5334.
[230] C. Xuan, et al., Composition-dependent electrocatalytic activities of NiFe-based selenides for the oxygen evolution reaction, Electrochim. Acta 291 (2018) 64–72.
[231] Z. Zou, et al., An Fe-doped nickel selenide nanorod/nanosheet hierarchical array for efficient overall water splitting, J. Mater. Chem. 7 (5) (2019) 2233–2241.
[232] K. Karthick, et al., Advanced Cu3Sn and selenized Cu3Sn@Cu foam as electrocatalysts for water oxidation under alkaline and near-neutral conditions, Inorg. Chem. 58 (14) (2019) 9490–9499.
[233] C. Zhang, et al., Self-supported iron-doping NiSe2 nanowrinkles as bifunctional electrocatalysts for electrochemical water splitting, J. Alloys Compd. 818 (2020) 152833.
[234] S. Anantharaj, S. Noda, Nickel selenides as pre-catalysts for electrochemical oxygen evolution reaction: a review, Int. J. Hydrogen Energy 45 (32) (2020) 15763–15784.
[235] E. Vayner, et al., Experimental and theoretical study of cobalt selenide as a catalyst for O2 electroreduction, J. Phys. Chem. C 111 (28) (2007) 10508–10513.
[236] C. Xia, et al., Selenide-based electrocatalysts and scaffolds for water oxidation applications, Adv. Mater. 28 (1) (2016) 77–85.
[237] Z. Fang, et al., Metallic transition metal selenide holey nanosheets for efficient oxygen evolution electrocatalysis, ACS Nano 11 (9) (2017) 9550–9557.
[238] Y. Choquette, H. Ménard, L. Brossard, Electrocatalytic performance of composite-coated electrodes for alkaline water electrolysis, Int. J. Hydrogen Energy 15 (1) (1990) 21–26.
[239] G. Barati Darband, M. Aliofkhazraei, A.S. Rouhaghdam, Facile electrodeposition of ternary Ni-Fe-Co alloy nanostructure as a binder free, cost-effective and durable electrocatalyst for high-performance overall water splitting, J. Colloid Interface Sci. 547 (2019) 407–420.
[240] E. Potvin, L. Brossard, Electrocatalytic activity of Ni-Fe anodes for alkaline water electrolysis, Mater. Chem. Phys. 31 (4) (1992) 311–318.
[241] F.J. Pérez-Alonso, et al., Ni/Fe electrodes prepared by electrodeposition method over different substrates for oxygen evolution reaction in alkaline medium, Int. J. Hydrogen Energy 39 (10) (2014) 5204–5212.
[242] F.J. Pérez-Alonso, et al., Ni–Co electrodes prepared by electroless-plating deposition. A study of their electrocatalytic activity for the hydrogen and oxygen evolution reactions, Int. J. Hydrogen Energy 40 (1) (2015) 51–61.
[243] F. Rosalbino, et al., Electrocatalytic activity of crystalline Ni–Co–M (M = Cr, Mn, Cu) alloys on the oxygen evolution reaction in an alkaline environment, Int. J. Hydrogen Energy 38 (25) (2013) 10170–10177.
[244] J.M. Jaksic, et al., Electrocatalysis for hydrogen electrode reactions in the light of fermi dynamics and structural bonding FACTORS—I. individual electrocatalytic properties of transition metals, Int. J. Hydrogen Energy 23 (12) (1998) 1121–1156.
[245] B.M. Jović, et al., Kinetics of the oxygen evolution reaction on NiSn electrodes in alkaline solutions, J. Electroanal. Chem. 754 (2015) 100–108.
[246] V.D. Jović, et al., Accelerated service life test of electrodeposited NiSn alloys as bifunctional catalysts for alkaline water electrolysis under industrial operating conditions, J. Electroanal. Chem. 819 (2018) 16–25.
[247] S.M. Fernández-Valverde, et al., Electrochemical behavior of Ni-Mo electrocatalyst for water electrolysis, J. Mexican Chem. Soc. 54 (3) (2010) 169–174.
[248] K. Yin, et al., A Bi2Te3@CoNiMo composite as a high performance bifunctional catalyst for hydrogen and oxygen evolution reactions, J. Mater. Chem. 3 (45) (2015) 22770–22780.
[249] Y. Cheng, et al., Pristine carbon nanotubes as non-metal electrocatalysts for oxygen evolution reaction of water splitting, Appl. Catal. B Environ. 163 (2015) 96–104.
[250] M. Gong, et al., An advanced Ni–Fe layered double hydroxide electrocatalyst for water oxidation, J. Am. Chem. Soc. 135 (23) (2013) 8452–8455.
[251] X. Lu, C. Zhao, Highly efficient and robust oxygen evolution catalysts achieved by anchoring nanocrystalline cobalt oxides onto mildly oxidized multiwalled carbon nanotubes, J. Mater. Chem. 1 (39) (2013) 12053–12059.
[252] M.P. Suryawanshi, et al., Hierarchically coupled Ni:FeOOH nanosheets on 3D N-doped graphite foam as self-supported electrocatalysts for efficient and durable water oxidation, ACS Catal. 9 (6) (2019) 5025–5034.
[253] B. Jeong, et al., The influence of a fibrous carbon envelope on the formation of CoFe nanoparticles for durable electrocatalytic oxygen evolution, Phys. Chem. Chem. Phys. 16 (27) (2014) 13807–13813.
[254] J. Wang, et al., Cobalt nanoparticles encapsulated in nitrogen-doped carbon as a bifunctional catalyst for water electrolysis, J. Mater. Chem. 2 (47) (2014) 20067–20074.
[255] K. Zhang, et al., N-doped CoO nanowire arrays as efficient electrocatalysts for oxygen evolution reaction, J. Energy Chem. 37 (2019) 13–17.
[256] H. Jin, et al., In situ cobalt–cobalt oxide/N-doped carbon hybrids as superior bifunctional electrocatalysts for hydrogen and oxygen evolution, J. Am. Chem. Soc. 137 (7) (2015) 2688–2694.
[257] X. Wu, et al., Metal-support interaction boosted electrocatalysis of ultrasmall iridium nanoparticles supported on nitrogen doped graphene for highly efficient water electrolysis in acidic and alkaline media, Nano Energy 62 (2019) 117–126.
[258] H. Liu, et al., Ultrathin Co 9 S 8 nanosheets vertically aligned on N,S/rGO for low voltage electrolytic water in alkaline media, Sci. Rep. 9 (1) (2019) 1951.
[259] J.R. Varcoe, et al., Anion-exchange membranes in electrochemical energy systems, Energy Environ. Sci. 7 (10) (2014) 3135–3191.
[260] W. Wang, J. Luo, S. Chen, Carbon oxidation reactions could misguide the evaluation of carbon black-based oxygen-evolution electrocatalysts, Chem. Commun. 53 (84) (2017) 11556–11559.
[261] F. Moureaux, et al., Timely-activated 316L stainless steel: a low cost, durable and active electrode for oxygen evolution reaction in concentrated alkaline environments, Appl. Catal. B Environ. 258 (2019) 117963.
[262] C. Schoeberl, M. Manolova, R. Freudenberger, Sol-gel-deposited cobalt and nickel oxide as an oxygen evolution catalyst in alkaline media, Int. J. Hydrogen Energy 40 (35) (2015) 11773–11778.
[263] Y. Meng, et al., Structure–property relationship of bifunctional MnO2 nanostructures: highly efficient, ultra-stable electrochemical water oxidation and oxygen reduction reaction catalysts identified in alkaline media, J. Am. Chem. Soc. 136 (32) (2014) 11452–11464.
[264] L. Fu, et al., IrW nanobranches as an advanced electrocatalyst for pH-universal overall water splitting, Nanoscale 11 (18) (2019) 8898–8905.
[265] S.M. Galani, et al., Development of RuO2/CeO2 heterostructure as an efficient OER electrocatalyst for alkaline water splitting, Int. J. Hydrogen Energy 45 (37) (2019) 18635–18644.
[266] H. Zhang, et al., Rapid low-temperature synthesis of hollow CuS0.55 nanoparticles for efficient electrocatalytic water oxidation, Chem. Eng. Sci. 195 (2019) 665–670.
[267] M. Dincă, Y. Surendranath, D.G. Nocera, Nickel-borate oxygen-evolving catalyst that functions under benign conditions, Proc. Nat. Acad. Sci. USA 107 (23) (2010) 10337–10341.
[268] X. Ren, et al., Cobalt–borate nanowire array as a high-performance catalyst for oxygen evolution reaction in near-neutral media, J. Mater. Chem. 5 (16) (2017) 7291–7294.
[269] J. Xie, et al., Zirconium trisulfide ultrathin nanosheets as efficient catalysts for water oxidation in both alkaline and neutral solutions, Inorg. Chemist. Front. 1 (10) (2014) 751–756.
[270] M. Ďurovič, J. Hnát, K. Bouzek, Electrocatalysts for the hydrogen evolution reaction in alkaline and neutral media. A comparative review, J. Power Sources 493 (2021), 229708.
[271] R. Frydendal, et al., Benchmarking the stability of oxygen evolution reaction catalysts, Import. Monitor. Mass Losses 1 (12) (2014) 2075–2081.
[272] X. Hu, et al., Nickel-iron selenide polyhedral nanocrystal with optimized surface morphology as a high-performance bifunctional electrocatalyst for overall water splitting, Appl. Surf. Sci. 488 (2019) 326–334.
[273] M.E.G. Lyons, S. Floquet, Mechanism of oxygen reactions at porous oxide electrodes. Part 2 - oxygen evolution at RuO2, IrO2 and Irx-Ru1-xO2 electrodes in aqueous acid and alkaline solution, Phys. Chem. Chem. Phys. 13 (12) (2011) 5314–5335.
[274] Z. Wu, et al., A Co-doped Ni–Fe mixed oxide mesoporous nanosheet array with low overpotential and high stability towards overall water splitting, J. Mater. Chem. 6 (1) (2018) 167–178.
[275] H.B. Tao, et al., Revealing energetics of surface oxygen redox from kinetic fingerprint in oxygen electrocatalysis, J. Am. Chem. Soc. 141 (35) (2019) 13803–13811.
[276] B. Kim, et al., Atomistic investigation of doping effects on electrocatalytic properties of cobalt oxides for water oxidation, Adv. Sci. (Weinheim, Baden-Wurttemberg, Germ.) 5 (12) (2018), 1801632-1801632.
[277] V. Fidelsky, M.C. Toroker, The secret behind the success of doping nickel oxyhydroxide with iron, Phys. Chem. Chem. Phys. 19 (11) (2017) 7491–7497.
[278] M.A. Oliver-Tolentino, et al., An approach to understanding the electrocatalytic activity enhancement by superexchange interaction toward OER in alkaline media of Ni–Fe LDH, J. Phys. Chem. C 118 (39) (2014) 22432–22438.
[279] X. Yu, et al., A high-performance three-dimensional Ni–Fe layered double hydroxide/graphene electrode for water oxidation, J. Mater. Chem. 3 (13) (2015) 6921–6928.
[280] R. Palkovits, S. Palkovits, Using artificial intelligence to forecast water oxidation catalysts, ACS Catal. 9 (9) (2019) 8383–8387.